

Oil & Natural Gas Technology

DOE Award No.: DE-FE0001243

Clean and Secure Energy from Domestic Oil Shale and Oil Sands Resources

Quarterly Progress Report (October - December 2010)

Submitted by:
Institute for Clean and Secure Energy
155 S. 1452 E. Room 380
Salt Lake City, Utah 84112

Prepared for:
United States Department of Energy
National Energy Technology Laboratory

February 15, 2010



Office of Fossil Energy

Clean and Secure Energy from Domestic Oil Shale and Oil Sands Resources

DOE Award No.: DE-FE0001243

Quarterly Progress Report

October 2010 to December 2010

Submitted by:
Institute for Clean and Secure Energy
155 S. 1452 E. Room 380
Salt Lake City, UT 84112

Principal Investigator: Philip J. Smith
Project Period: October 1, 2009 to March 31, 2011

Prepared for:
U.S. Department of Energy
National Energy Technology Laboratory

Acknowledgment: "This material is based upon work supported by the Department of Energy under Award Number DE-FE0001243."

Disclaimer: "This report was prepared as an account of work sponsored by an agency of the United States Government. Neither the United States Government nor any agency thereof, nor any of their employees, makes any warranty, express or implied, or assumes any legal liability or responsibility for the accuracy, completeness, or usefulness of any information, apparatus, product, or process disclosed, or represents that its use would not infringe privately owned rights. Reference herein to any specific commercial product, process, or service by trade name, trademark, manufacturer, or otherwise does not necessarily constitute or imply its endorsement, recommendation, or favoring by the United States Government or any agency thereof. The views and opinions of authors expressed herein do not necessarily state or reflect those of the United States Government or any agency thereof."

EXECUTIVE SUMMARY

The Clean and Secure Energy from Domestic Oil Shale and Oil Sands Resources program is part of the research agenda of the Institute for Clean and Secure Energy (ICSE) at the University of Utah. In this quarter, the Clean and Secure Energy program circulated External Advisory Board recommendations and began the transfer of the ICSE repository to the digital collections of the University of Utah's Marriott Library.

In Task 3.0, ICSE researchers developed an Excel tool for estimating life-cycle GHG emissions from the Promax models developed under Subtask 6.1. Results from the simulation of an oxy-gas burner show the internal and external recirculation zones characteristic of the flame from the ENEL TEA-C burner. Based on these results, there is a clear need to include swirl as an inlet boundary condition for both the primary and secondary/tertiary recycled flue gas + O₂ streams.

In Task 4.0, ICSE researchers are wrapping up work in this phase of the project as they are anxious to bring a more integrated approach in the next phase using the Skyline 16 core sample as the means of integration. The Subtask 4.1 team used DEM simulations in Star-CCM+ to create complex geometries involving on the order of a hundred pieces of shale. A sixty-two piece oil shale particle simulation has shown capability in modeling the transient fluid flow and heat transfer phenomena that occur in a heated oil shale bed. The Subtask 4.2 team completed core descriptions for the P-4 and Coyote Wash 1 cores and a regional cross-section. For the simulation portion of the subtask, initial simulations of an in situ oil shale production process did not produce significant oil because of heat transfer limitations. These limitations were resolved by decreasing the well spacing, suggesting that with probable oil shale reservoir conditions (low permeability, low heat conductivity), there is an upper limit to the well spacing. The Subtask 4.3 team obtained results from two different scales of oil shale pyrolysis experiments ($\frac{3}{4}$ " and 2.5" cores). Chromatograms taken of the oil produced during the experiments indicate that compositionally, the two oils were very similar. The next step is to perform the same type of experiments under stress, so an apparatus was designed for this purpose. The Subtask 4.4 team produced water from the pyrolysis of a 2.5" diameter oil shale core sample and then sent the water to a laboratory for analysis. All volatile and semi-volatile hydrocarbon compounds were below detection limits. The Subtask 4.5 team modeled pore network structure at different heating rates to determine porosity changes and used multiphase LB model to analyze fluid penetration into porous samples such as pyrolyzed oil shale and oil sands. Subtask 4.6 researchers calculated chemical shifts obtained for six different asphaltene structures, demonstrating that NMR is sensitive to the differing structural features of the models.

In Task 5.0, ICSE researchers completed two Topical Reports, one focused on land use issues associated with potential development of oil sands and oil shale and the other focused on produced water. Both reports will be uploaded to OSTI after approval from the DOE-NETL Program Manager.

In Task 6.0, ICSE researchers focused on the completing the first five sections of the draft Market Assessment report and revising the engineering and economic analyses for the three in situ development scenarios to include horizontal drilling as an option. In addition, researchers completed research and analysis related to taxes and royalties levied on oil sands production, as well as downstream and marketing challenges facing oil sands development. This research will be included in the Oil Sand Topical Report.

PROGRESS, RESULTS, AND DISCUSSION

Task 1.0 - Project Management and Planning

During this quarter, there were no schedule/cost variances or other situations requiring updating/amending of the PMP.

Task 2.0 -Technology Transfer and Outreach

This task focuses on industry, academic and public outreach and education efforts, as well as implementing the External Advisory Board (EAB) recommendations. The final EAB recommendations, approved by EAB members last quarter, were circulated to ICSE faculty and staff. Preparations also were begun this quarter for the 2011 EAB meeting, and for the 2011 Energy Forum, at which former Governor Dave Freudenthal of Wyoming has agreed to be a speaker.

Task 2.0 work this past quarter has also focused on transitioning the ICSE Digital Repository and the Interactive Map, both of which have been defunded due to budget constraints. Wendy Ajax, the Institute Librarian, and Michelle Kline, the Institute GIS Specialist, terminated their employment with ICSE effective December 31, 2010.

The Marriott Library at the University of Utah has agreed to permanently house what are now the contents of the ICSE Digital Repository, and discussions are continuing with the library to see if a similar home can be found for the Interactive Map. Digital Repository efforts during the last quarter focused on (1) the addition of publications and other items into the repository in preparation for migration to the new collection that will be managed by the Marriott library and (2) development of the computer program needed to convert the export format of DSpace to a suitable input format for the Marriott Library's ContentDM. After a test import was conducted, the Marriott Library requested some export data modifications before the final export of the Digital Repository is delivered. The final migration should occur next quarter. Interactive Map work this past quarter focused on continued refinement of the Interactive Map's website statistics tools and continued monitoring of Interactive Map usage. Maintenance responsibilities for the Interactive Map were transferred from Michelle Kline to Terrance Davis, the Institute's Web Applications Programmer.

Two deliverables related to Task 2.0 were completed in this quarter. Utah Geological Survey (UGS) delivered a table of 300+ wells with average oil yield values for lower R-8, A-groove, Mahogany, B-groove, upper R-6, lower R-6, L-5, R-5, L-4, & R-4 zones in Uinta Basin, UT. UGS also completed GIS maps displaying thickness & richness of each oil shale zone and provided the maps to ICSE in both hard copy and CD form.

Task 3.0 - Clean Oil Shale and Oil Sands Utilization with CO₂ Management

Subtask 3.1 – Macroscale CO₂ Analysis (PI: Kerry Kelly, David Pershing)

During this quarter, the Project Team continued their evaluation of the life-cycle greenhouse gas (GHG) emissions for several of the air-fuel and oxy-fuel scenarios developed under Subtask 6.1. They also completed their milestone to develop an Excel tool for estimating life-cycle GHG emissions from the Promax models developed under Subtask 6.1.

Subtask 6.1 Promax results can be exported and inserted into an Excel file, which has been developed to quickly perform an analysis of GHG emissions. This file links to the key outputs:

electricity use, natural gas consumption, CO₂ emissions, etc. It also allows the user to select the appropriate electricity grid.

Of the processes evaluated by Subtask 6.1, ex situ production of transportation fuels from oil sands appears to be one of the most feasible. Figure 1 illustrates the processes included in an evaluation of GHG emissions from a Utah ex situ oil sands production scenario. Both conventional firing and oxyfiring with CO₂ capture in the various combustion processes associated with production, upgrading, and refining are evaluated.

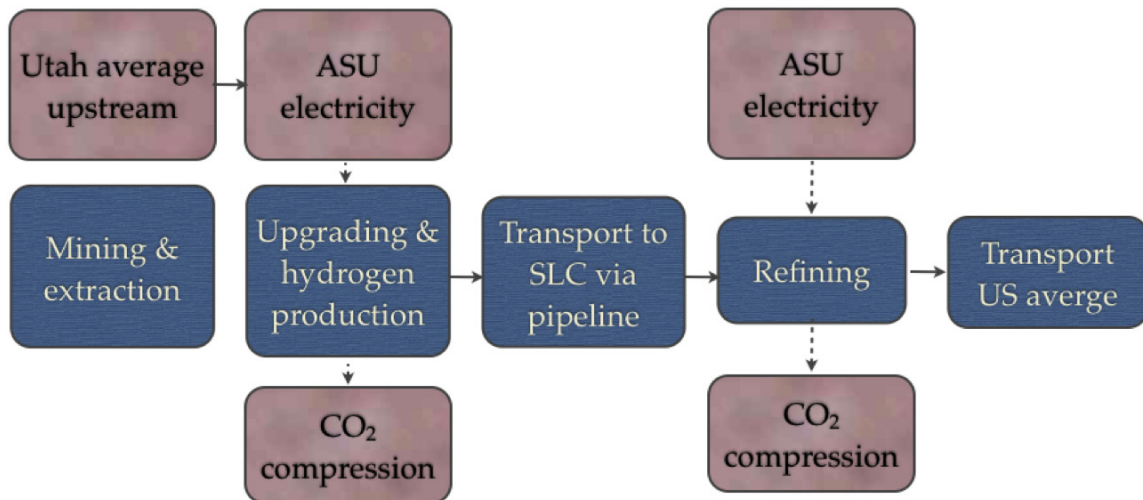


Figure 1: Processes included in an evaluation of GHG emissions generated from the ex situ production of transportation fuels from Utah oil sands. Processes noted in blue are included in both conventional and oxyfired scenarios, while tan boxes are only included in oxyfired scenarios.

Figure 2 illustrates the life-cycle GHG emissions from the ex situ production of gasoline from Utah oil sands. It clearly shows that oxyfiring with CO₂ capture reduces life-cycle GHG emissions. Although this analysis is preliminary, employing oxyfiring in the production, upgrading, and refining stages may bring Utah oil sands into the range of GHG emissions from conventional crude oil (see dotted line in Figure 2). Finally, the GHG emissions from the air-fired oil sands scenario are in the range of the values reported by other researchers (see error bar on Figure 2).

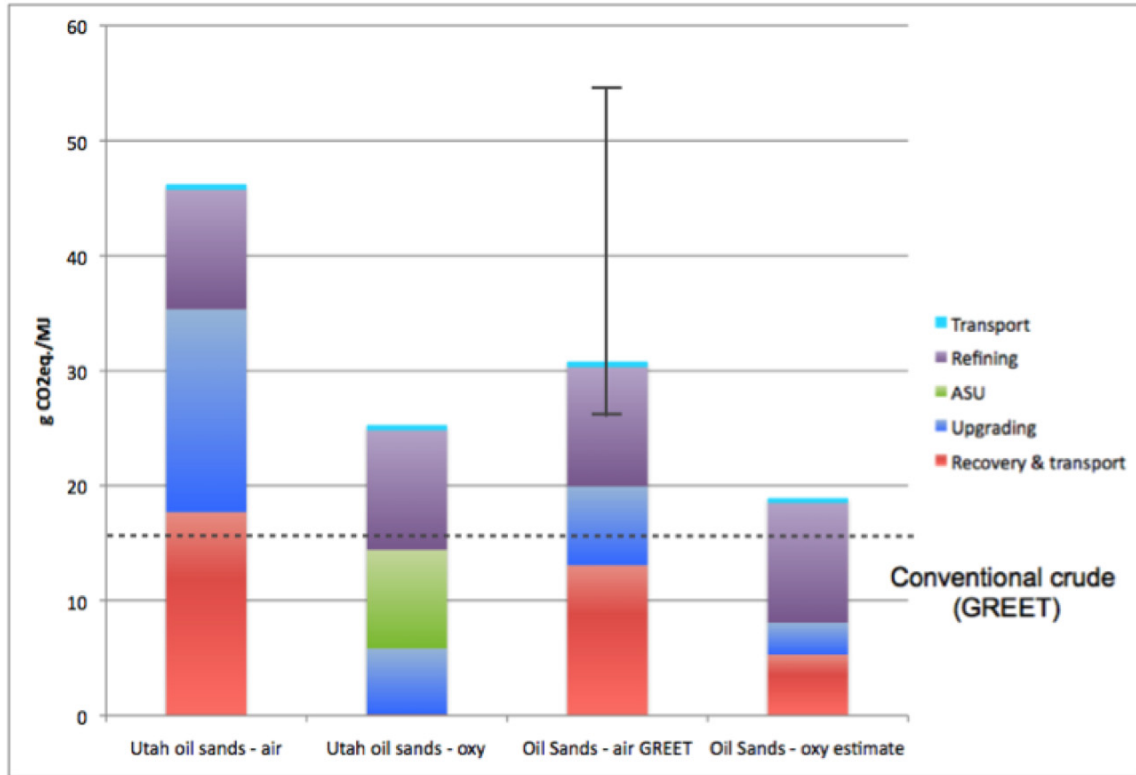


Figure 2: Life-cycle GHG emissions from the ex situ Utah oil sands scenario (air and oxy firing shown in first two bars). The oil sands-air GREET bar shows the life-cycle GHG emissions for ex situ Canadian oil sands obtained the GREET model; the error bar shows the range of emissions reported by other researchers. The final bar shows the oil sands – oxy estimate, which included oxyfiring in the refining stage with CO₂ capture. The dotted line indicates life-cycle GHG emissions from conventional crude oil as estimated by GREET.

Subtask 3.2 - Flameless Oxy-gas Process Heaters for Efficient CO₂ Capture (PI: Jennifer Spinti)

In this quarter, Subtask 3.2 researchers completed initial simulations of the oxy-gas experiments conducted by the International Flame Research Foundation (IFRF). Previous difficulties with code stability for these oxy-fired cases have been resolved; the problems were due to the way the reaction chemistry was read in by the Large Eddy Simulation (LES) code. A new oxy-gas table was created using Digital Analysis of Reaction Systems (DARS) software. With this table, a simulation of the IFRF furnace fired by the ENEL TEA-C burner was completed (Coraggio and Laiola, 2009).

For the simulation, the burner had three concentric injection ports. In the primary inlet, recycled flue gas (RFG) was injected into the furnace. In the annular gas ring, natural gas was injected. In the annular secondary/tertiary ring, recycled flue gas (RFG) mixed with O₂ was injected. The computational domain was 2m x 2m x 2m with a mesh resolution of 225 x 225 x 225. With this resolution, the burner inlets are reasonably resolved. All transport equations were solved with second order numerical schemes. Figure 3 shows a volume-rendered image of the temperature field while Figure 4 shows a similar image of the mixture fraction field. When mixture fraction of 0 (blue) represents pure oxygen while a mixture fraction of 1 (red) represents pure natural gas. In diffusion-type flames such as this one, the highest temperatures are found in the mixing zone

between the fuel and oxidant layers. The annular ring of natural gas (red) mixing with the oxidant can be clearly seen in Figure 4.

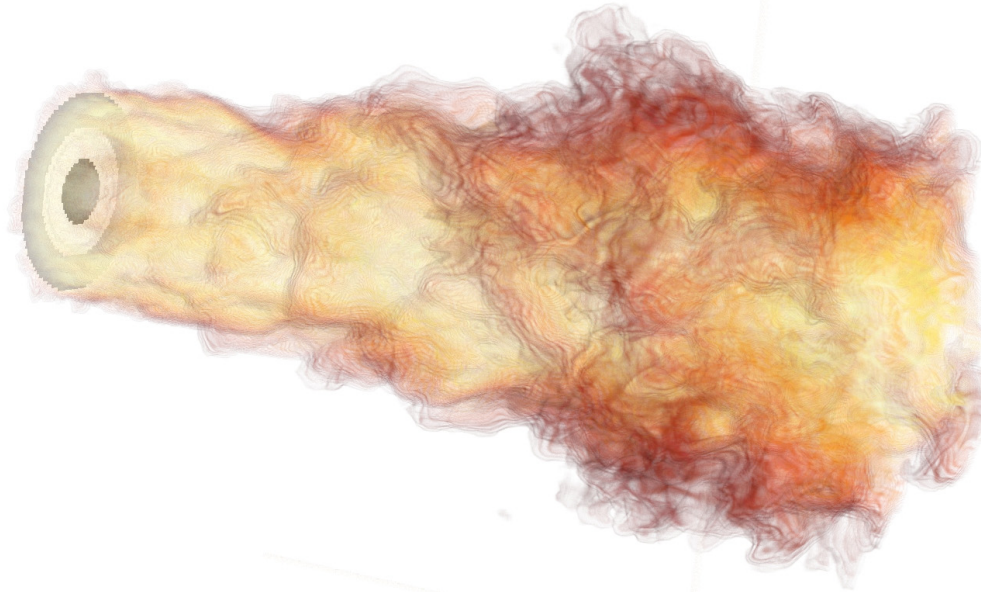


Figure 3: Volume-rendered image of temperature in oxy-gas flame in IFRF furnace fired with ENEL TEA-C burner.

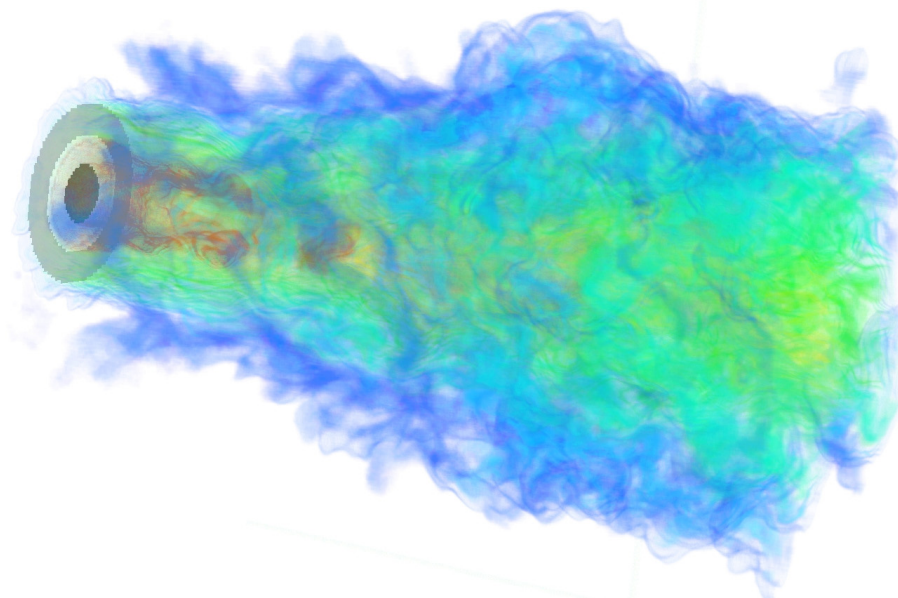
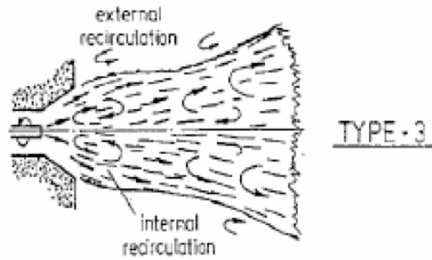


Figure 4: Volume-rendered image of mixture fraction in oxy-gas flame in IFRF furnace fired with ENEL TEA-C burner.

The IFRF has classified flames as type-0 through type-3. As noted by Coraggio and Laiola (2009), the flame in the oxy-gas cases is close to type-3, whose shape and characteristics are shown in Figure 5. This flame is characterized by both internal and external recirculation. From a qualitative standpoint, the vorticity field from the simulated flame shown in Figure 6 resembles the type-3 flame. A view of 2D slices through the vorticity field reveals strong recirculation regions between the primary jet and annular gas jet and also along the edges of the secondary/tertiary jet.



- intense but longer flames on the quart with two internal recirculation zones
- can be produced with very high combustion air swirl and a high furnace confinement
- rarely found in industrial situations

Figure 5: Characteristics of IFRF type-3 flame (from Coraggio and Laiola, 2009).

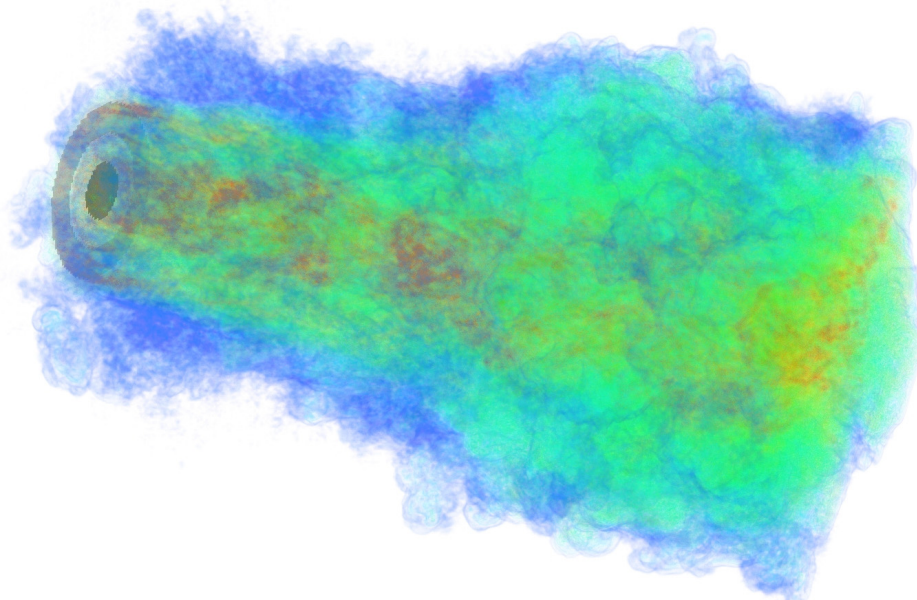


Figure 6: Volume-rendered vorticity field in oxy-gas flame in IFRF furnace fired with ENEL TEA-C burner.

This task had a milestone this quarter of a preliminary report detailing results of skeletal validation/uncertainty quantification (V/UQ) analysis of oxy-gas combustion system. Due to the

unforeseen coding problems mentioned previously and the computing resources issue addressed in the previous quarterly report, researchers were unable to complete the V/UQ analysis during this past quarter. To complete the requisite analysis, two additional capabilities need to be added to the LES code. The first is the ability to include swirl as part of the inlet boundary condition. The ENEL TEA-C burner has swirl vanes in both the primary and secondary/tertiary streams. While Coraggio and Laiola (2009) did not directly measure the velocity components at the burner inlet, the swirl number clearly had an effect on their flame profiles (e.g. temperature, CO₂ and O₂ concentrations, etc.) The impact of swirl on the mixing in the near-burner region is one parameter that has been added to the test matrix as a result of these initial simulations. A second capability is the implementation of flamelets-type reaction models. This implementation requires that reaction chemistry be tabulated with an additional independent variable, scalar dissipation rate; the other independent variables are mixture fraction and heat loss. Researchers are currently working to implement these models so that the desired test matrix can be executed.

Task 4.0 - Liquid Fuel Production by In-situ Thermal Processing of Oil Shale/Sands

Subtask 4.1 - Development of CFD-based Simulation Tools for In-situ Thermal Processing of Oil Shale/Sands (PI: Philip Smith)

Using the commercial software Star-CCM+, Subtask 4.1 researchers are developing a high performance computing (HPC), computational fluid dynamics (CFD)-based, heat transfer simulation for in-situ thermal processing of oil shale. In this quarter, researchers have implemented a new method for representing shale particles inside the computational domain. The new method presents two main advantages over the previous approach:

1. It helps to preserve the particle local coordinate system, which is important for implementation of directional properties of the oil shale.
2. It produces smooth edges for an improved computational mesh.

Additionally, in conjunction with their industrial partners, Subtask 4.1 researchers have refined their research objectives, identified the computational challenges associated with that objective, and revised their milestones and subtask deliverable.

Milestone plan/status and revised deliverable

- *Implement submodels for pyrolysis, porosity development, etc. that provide stable solution (milestone 4.2)*- In discussions with both Red Leaf Resources and Uintah Partners, Subtask 4.1 researchers has been told that heat transfer to the shale is the critical information that simulation can provide. These companies are specifically interested in the time history of the heating of each of the shale elements. Hence, researchers are focused on demonstrating that HPC simulations can answer this question in ways that field experiments alone cannot. The questions regarding subsequent yield can be incorporated later, when the models for pyrolysis and porosity development become available from other subtasks. Consequently, researchers propose to modify this milestone to be that of obtaining a time-temperature history for all oil shale elements with a milestone completion date of the end of March 2011.
- *Revised deliverable*- As discussed below, Subtask 4.1 researchers propose the following revision in to their subtask deliverable: A topical report detailing the heat transfer process inside the representative computational geometry. This revised deliverable will address the most urgent needs of Red Leaf Resources and will increase the research collaboration with our industrial partner for a rapid deployment of new technology.

In the previous quarterly report, Subtask 4.1 researchers addressed issues related to creating a valid mesh for a proper fluid flow simulation. Sharp edges on each piece of oil shale produce flow-field meshing problems. Consequently, researchers have been exploring several methods for decreasing the geometric complexity of the mesh to reduce the number of highly skewed mesh elements. They previously explored and reported on the wrapped surface geometry model, which was used to smooth the sharp corners. However, this model has created new difficulties in preserving independent pieces of oil shale. They have also explored a reduction in the size of the computational elements to refine all sharp geometries, which led to an excessive number of computational cells. Additionally, neither of these methods addressed a second vexing problem: that of the presence of internal gas volumes trapped among multiple pieces of shale. These regions create independent flow domains that cannot be solved simultaneously with the open flow channels.

Subtask 4.1 researchers have now developed a two-pronged strategy. First, they will circumvent these problems by simplifying the shale geometry, allowing the rapid completion of a fully coupled heat-transfer simulation. Second, they will retain the complex geometry and explore methods for resolving the meshing difficulties. This approach has a higher probability of meeting the industrial partner's needs (Red Leaf Resources) in a shorter time period.

The new strategy for rapid prototyping of the overall simulation process involves using tools available in the newest version of Star-CCM+ software, namely the Discrete Element Method (DEM) model. With this tool, the oil shale bed geometry has been developed in a simplified form. Investigation of the new model and its capabilities led to the creation of a sixty-two particle geometry consisting of spherically grouped elements. A simplified particle representing a single piece of oil shale is shown in Figure 7.

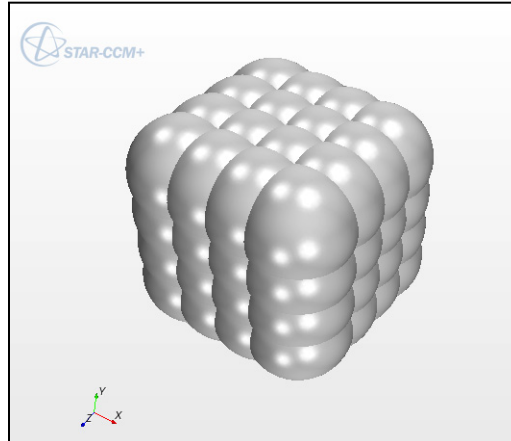


Figure 7: DEM shape formed from a grouping of spheres in Star-CCM+ used to show a simplified representation of one piece of oil shale.

This approach is beneficial in two ways. First, since all particles are created in Star-CCM+, the representation of each oil shale particle can maintain distinct identity and directional property in the simulation. Second, the geometry contains no intersections and sharp transitions, thus decreasing the difficulty of applying a more appropriate mesh. The decreased effort in creating a more suitable mesh for the flow and heat transfer simulation allows researchers to move more rapidly toward obtaining a thermal profile inside the representative computational domain.

In order to demonstrate the new DEM capabilities, Subtask 4.1 researchers first created a simplified computational geometry domain containing sixty-two particles, as shown in Figure 8. These particles are uniform in size and are distributed evenly throughout the inlet of the domain. After the DEM simulation was completed, the process of taking the simulation data and creating a computer-aided-design (CAD) of the geometry was done using Matlab and Star-CCM+. The new geometry was meshed in Star-CCM+ using the surface wrapping model and a polyhedral volume mesh, resulting in a mesh of 3.5 million cells. Because of the rounded edges on each particle, the meshing was a straightforward process. This rapid prototyping with DEM does not allow for a realistic oil shale particle size distribution. Methods developed, demonstrated and discussed in the previous quarterly reports show how realistic shale geometries that occur in field experiments can be obtained. This issue will be further addressed in the next quarterly report.

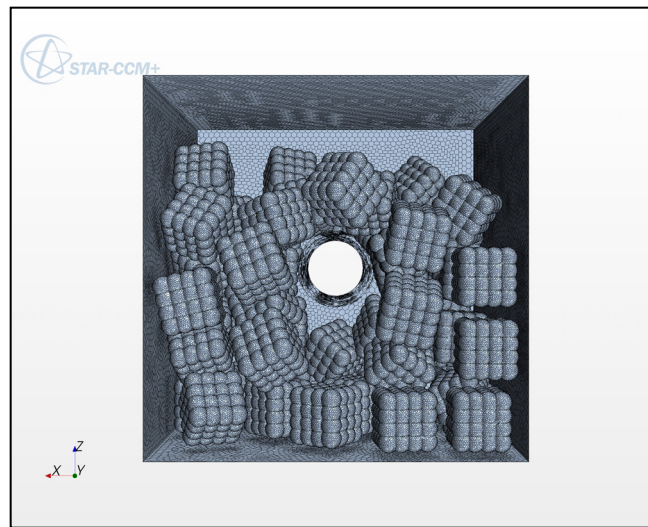


Figure 8: Image of the surface mesh created for the oil shale simulation bed in Star-CCM+.

Fully transient flow simulations with heat transfer to both the fluid and solid phases were performed on the simplified geometry. Figures 9 and 10 show the velocity vectors in a plane within the geometry and the temperature profile in the shale and fluid regions at 22.5 minutes of simulation time. Results appear as expected, yielding an upward buoyant plume of hot air, interacting with the geometry and mixing throughout the domain. The pieces of shale in the pathway of the convective current of hot air show increased heating. For this simulation, simplified shale properties were used that do not necessarily represent the properties of the oil shale used by our industrial partner. Nonetheless, the stable simulation demonstrates that researchers are able to produce a stable simulation with the expected thermal profile.

After obtaining a stable computational simulation with the simplified geometry domain, researchers created a domain that contains about 2000 particles, shown in Figure 11, to test the ability of Star-CCM+ to generate and handle large amounts of particles. They have noticed increased memory demands by the software, which continuously cause it to terminate its execution, and are trying to determine whether this is a software or a hardware limitation.

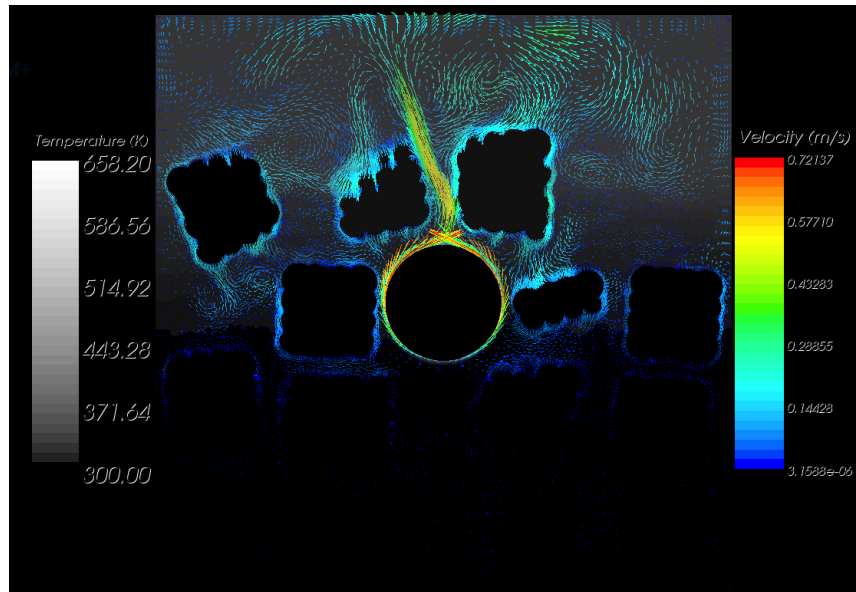


Figure 9: Velocity vectors in a plane inside the domain for the laminar simulation.

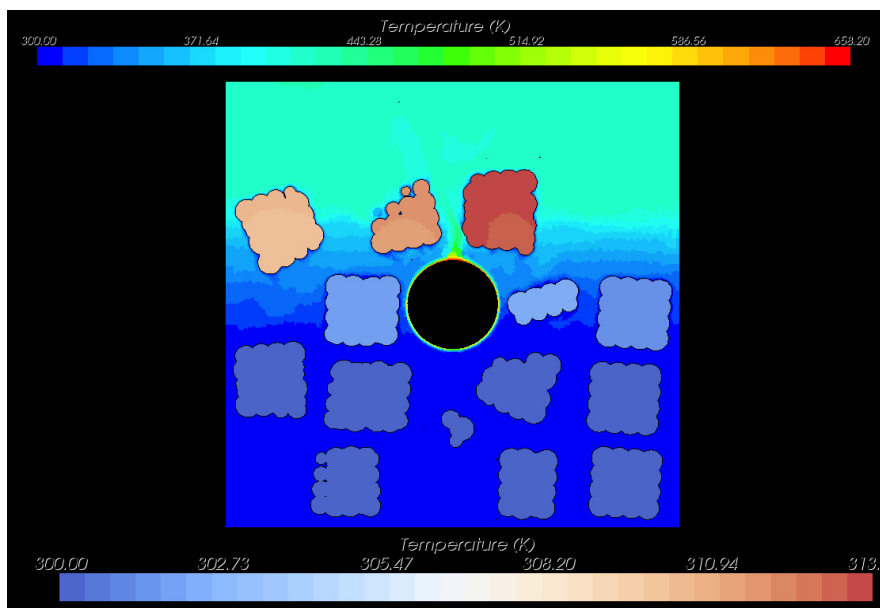


Figure 10: Temperature profile in both oil shale and fluid regions in a plane inside of the computational domain for the laminar simulation.

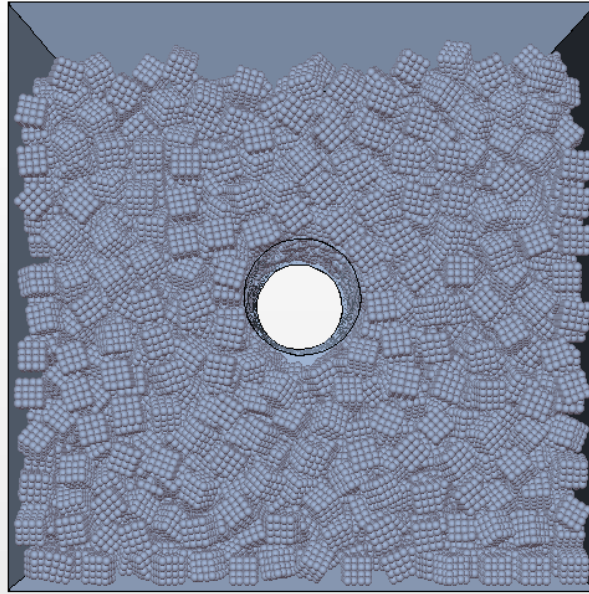


Figure 11: 2000+ particle geometry created for oil shale simulation.

Subtask 4.1 researchers are also creating a computational geometry which is more representative of the actual geometry used by Red Leaf Resources. This geometry is shown in Figure 12. With this geometry, they will perform a full flow and thermal simulation in the next quarter.

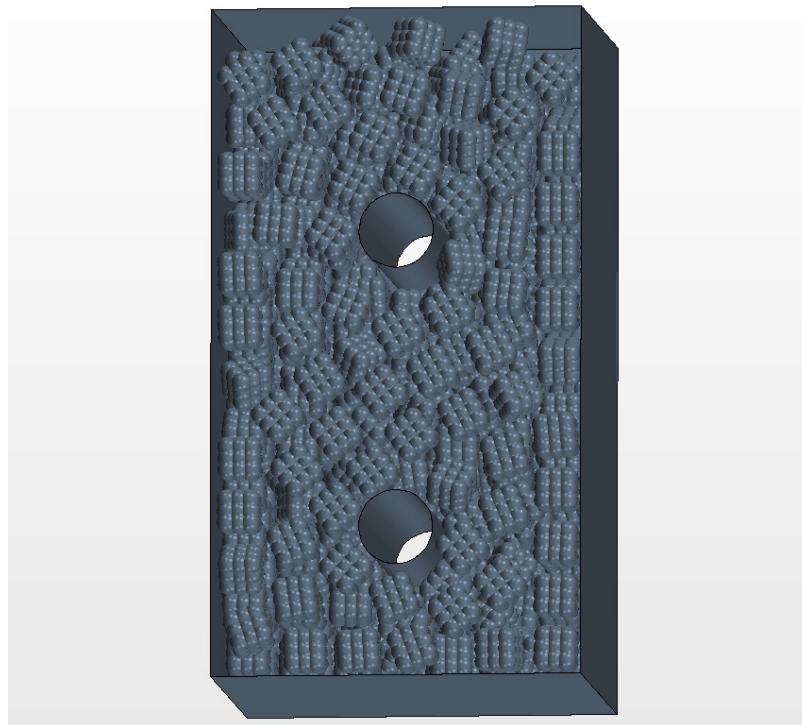


Figure 12: New computational domain geometry that more closely resembles the test bed geometry used by Red Leaf Resources to conduct their field experiment.

The DEM simulations in Star-CCM+ have shown success in creating complex geometries involving on the order of hundred pieces of shale. Especially significant is the new method of creating the rubblized shale geometry, which does not present many difficulties for proper meshing of the computational domain. A sixty-two piece oil shale particle simulation has shown capability in modeling the transient fluid flow and heat transfer phenomena that occur in a heated oil shale bed. Creation of a representative geometry that more closely resembles the experimental geometry used by Red Leaf Resources is currently under way.

Subtask 4.2 - Basin-wide Characterization of Oil Shale Resource in Utah and Examination of In-situ Production Models (PI: Milind Deo)

During this quarter, the Project Team completed the two project milestones with due dates of December 2010. Both milestones were related to the characterization of the oil shale resource in Utah. Core descriptions for both the P-4 and Coyote Wash 1 cores were completed. Team members also reexamined the Utah State 1 core, focusing on a more detailed description of the paleontology and sedimentary features in order to better compare it with the other cores. The regional cross-section is also finished and the Project Team is currently working on a synthesis report to be completed by early March 2011.

For the simulation part of the project, the Project Team has approached the challenge of garnering relevant information from complex in situ oil shale modeling by using experimental design techniques. In situ oil shale simulations are complex because chemical kinetics, heat transfer, phase behavior, geomechanical dynamics, and multiphase flow are all pertinent physical processes occurring over a wide range of time and length scales. Experimental design techniques are useful for exposing dominant parameters (and dominant interactions between parameters) in simulations for predicting an outcome of interest. After dominant parameters are exposed, simpler surrogate models, or response surfaces, can be used to estimate the results from detailed full simulations.

This concept was demonstrated by studying the following parameters in oil shale simulations: (1) Molecular weight of kerogen/stoichiometry/initial kerogen molar concentration (these values are treated as one parameter since they are dependent on each other to conserve volume and mass balances), (2)-(5) activation energies for reactions 1-4 in the kerogen pyrolysis mechanism shown below, (6) with/without normal distribution of activation energies for reaction 1, (7) relative permeability representation, and (8) reaction enthalpy.

Reaction 1 Kerogen \rightarrow HO + LO + gas + CH₄ + char
Reaction 2 HO \rightarrow LO + gas + CH₄ + char
Reaction 3 LO \rightarrow gas + CH₄ + char
Reaction 4 Gas \rightarrow CH₄ + char
Reaction 5 Char \rightarrow CH₄ + gas + coke

Initial simulations did not produce significant oil because of heat transfer limitations. These limitations were resolved by decreasing the well spacing from 53 feet to 26.5 feet (see Figure 13), suggesting that with probable oil shale reservoir conditions (low permeability, low heat conductivity), there is an upper limit to the well spacing. Otherwise, liquid oil will not be mobile and could further convert to gases and residual carbon species.

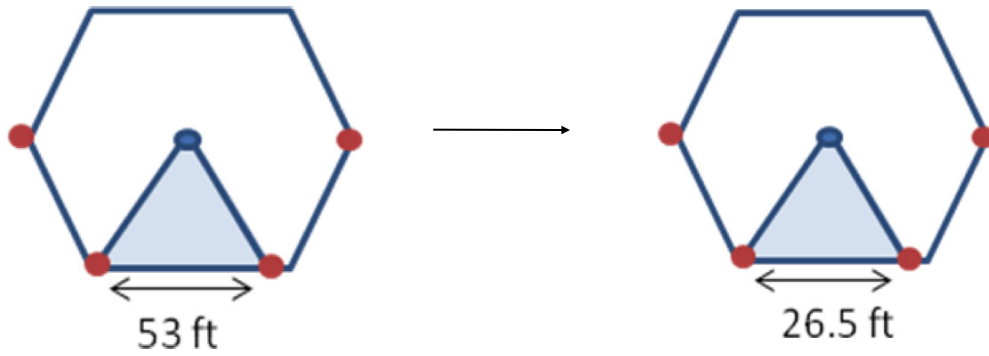


Figure 13: Aerial dimensions of the simulated heating (red) and production (blue) wells.

Results presented by Taciuk at the 29th Oil Shale Symposium at the Colorado School of Mines (2009) also suggest that excessive residence time of oil in the reservoir can impact the yield as shown in Figure 14.

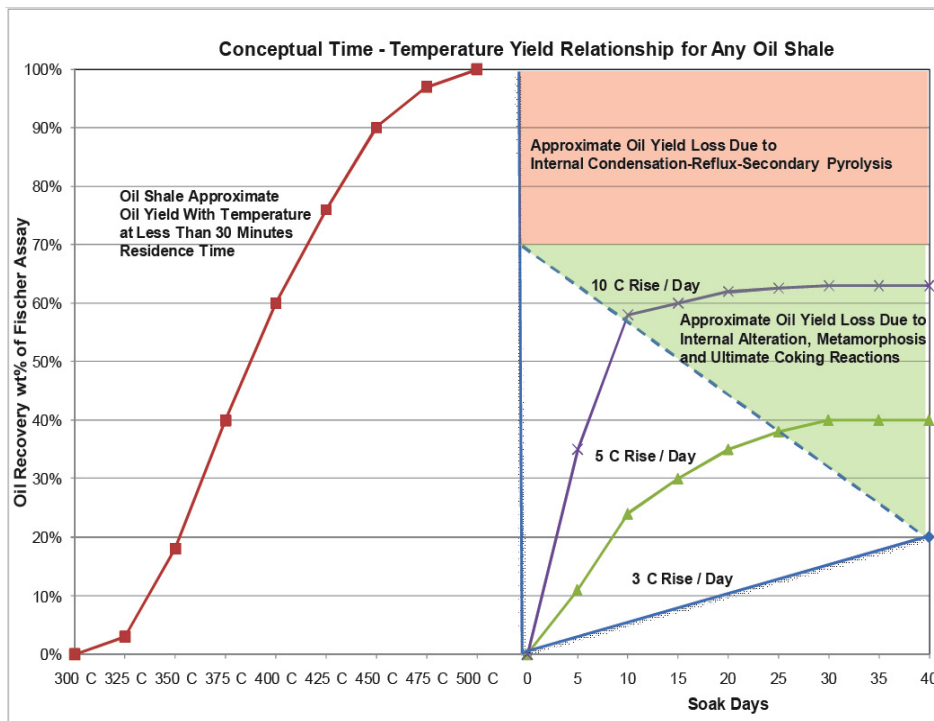


Figure 14: Time/temperature yield during oil shale pyrolysis (from Taciuk, 2009).

With the reduced well spacing, it was found that the parameters with the greatest impact on the ultimate recovery of oil were activation energy for kerogen pyrolysis, activation energy for oil decomposition to gas, a distribution of activation energies for kerogen pyrolysis, the relative permeability representation, and the interactions between these parameters. These parameters were used to create the following surrogate model.

$$y = \beta_o + \sum_{i=1}^k \beta_i x_i + \sum_{i \neq j}^k \sum \beta_{ij} x_i x_j + \sum \sum \sum_{i \neq j \neq l} \beta_{ijl} x_i x_j x_l + \beta_{ijklm} x_i x_j x_l x_m$$

This model was characterized with 3 validation runs and found to have about 15% error for predicting the results of a full simulation. Additionally, 80 000 random calculations were made with the surrogate model to estimate the uncertainty introduced due to variations in the significant input parameters. Figure 15 is a histogram showing the results of these calculations. The results are also compared with a normal distribution (red curve).

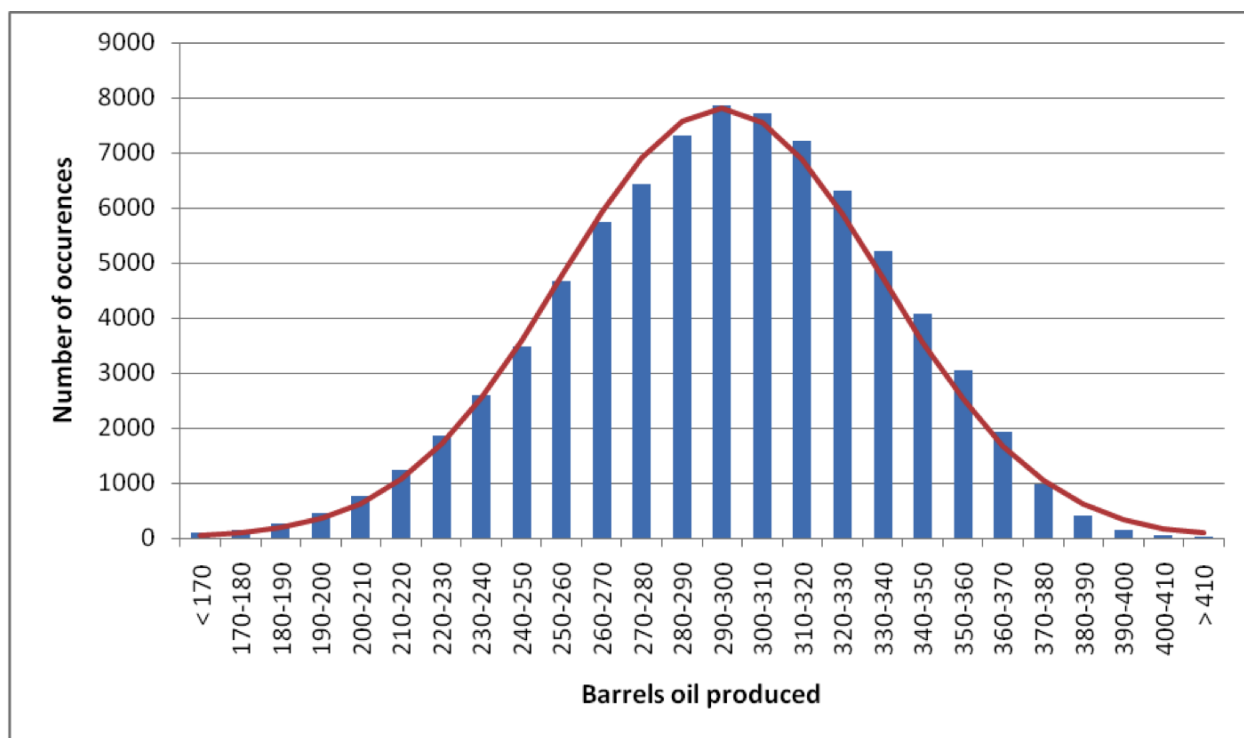


Figure 15: Histogram of oil production predicted from surrogate model using variable parameters.

Subtask 4.3 – Multiscale Thermal Processing of Oil Shale (PI: Milind Deo, Eric Eddings)

The Project Team has obtained results from two different scales of pyrolysis experiments with oil shale samples from the Green River Formation and has completed the last of the milestones related to this phase of the project with the design of the experiment for performing pyrolysis under stress. The experiments were performed with ¾” and 2.5” cores at 500°C and 500 psi for a duration of 24 hours. The schematic of the experimental setup and images of the ¾” core experiment are shown in Figure 16. Nitrogen was used to pressurize the reactors and to sweep the products. The pressure in the pyrolysis reactor system was maintained at 500 psi using a back pressure regulator (BPR). Temperatures at the surface and at the center of core were monitored and recorded. The surface temperature was used to control the pyrolysis temperature. The liquid product was collected and gaseous products escaped through the BPR to a series of condensers where the condensable compounds were collected. The temperature

of the condensers was maintained at -6°C . The oil product from all the units was collected, mixed and analyzed for the quality measurement. The gaseous products were collected in Tedlar bags. The gas sampling was done in the same bag at two stages: (1) when the reactor reached at desired temperature and (2) when the setup was unpressurized at the end of experiment. The gas mixture of these two stages was assumed to be a good average representative of the process.

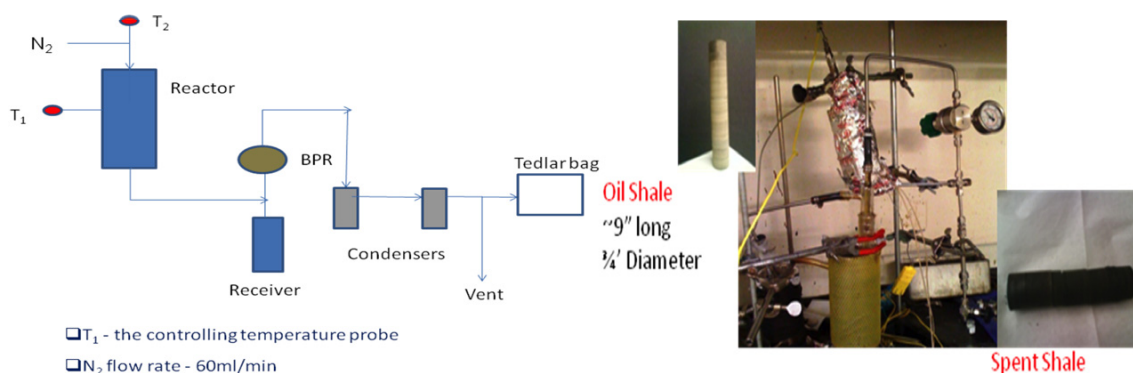


Figure 16: Schematic of the experimental setup and images of the $\frac{3}{4}$ " core pyrolysis at 500°C and 500 psi.

Overall mass balance- The distribution of pyrolysis products from experiments at these two different scales is summarized in Table 1. The percentage weight loss was higher for the 2.5" core pyrolysis compared to $\frac{3}{4}$ " core. However, the overall oil yield decreased and coke amount increased as the sample size increased, possibly due to secondary reactions in the oil/ vapor products and intraparticle mass transfer. The gas amount was estimated by the difference of the total weight loss and the oil and coke produced.

Table 1. Overall mass balance of pyrolysis products.

Results	2.5" core	$\frac{3}{4}$ " core
Wt loss %	24.52%	18.69%
Oil yield %	7.96%	10.63%
Coke %	4.14%	1.03%
Gas%	16.56%	8.06%
Unreacted organic%	0.05%	0.43%

Oil quality- The liquid and gas products were collected during the process and were analyzed using gas chromatography (GC). Gas chromatography was performed with a Restek MXT-1 column and an FID detector. Chromatograms for the oil produced from the 2.5" and $\frac{3}{4}$ " cores (with internal standard from C13-C18) are shown in Figures 17 and 18. The chromatograms indicate that compositionally, the two oils were very similar. To compare the quality of the oils produced, the chromatograms were classified based on single carbon number (SCN) distributions (plotted in Figure 19). The gas chromatograms and SCN distributions show that the quality of the oil produced at these two different scales is not much different. The peak differences reveal that the $\frac{3}{4}$ " sample has relatively more C10-C14 compounds while the 2.5" sample shows a distribution shift to C24-C26 compounds.

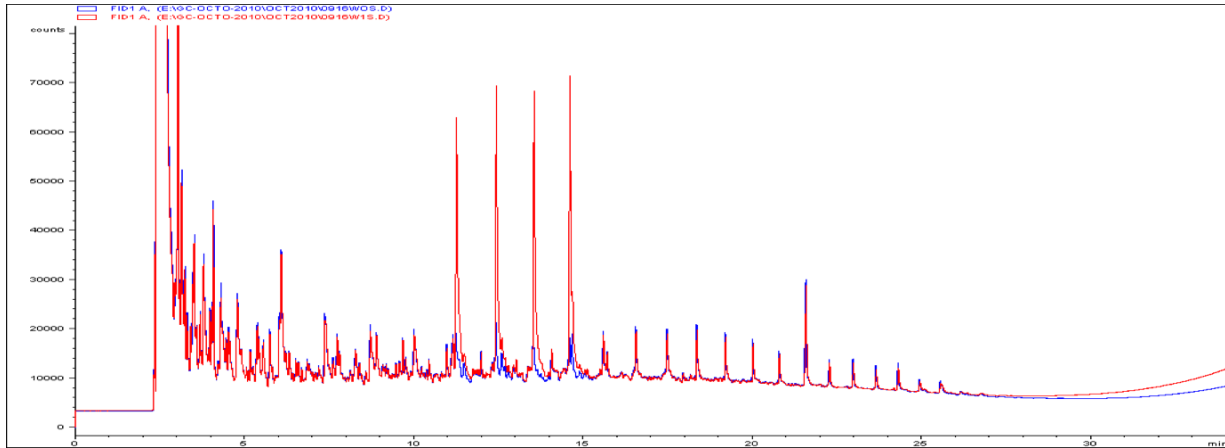


Figure 17: Chromatogram for oil produced from 2.5" core pyrolysis. The second chromatogram shown (red) is with the internal standard containing alkanes from C14-C18.

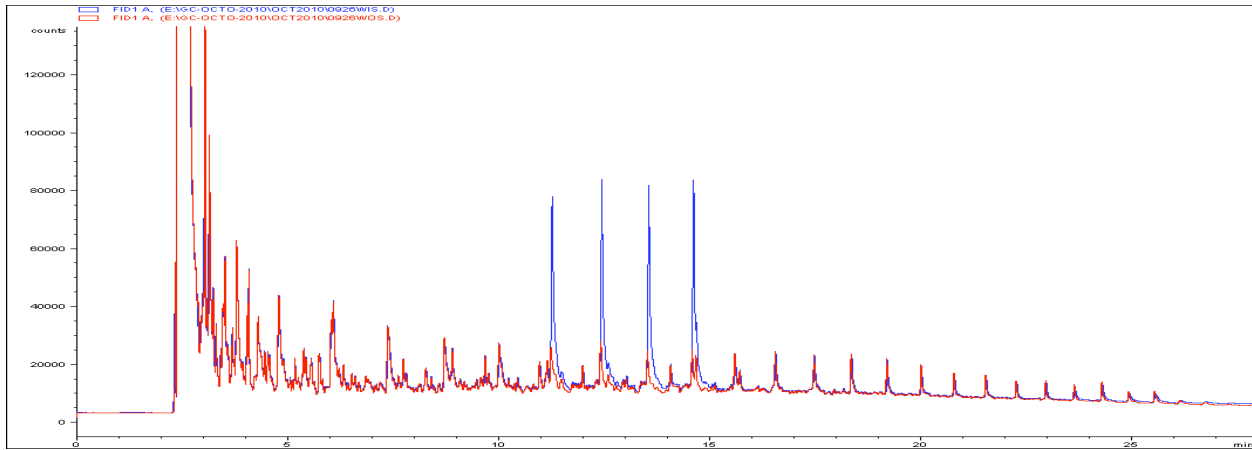


Figure 18: Chromatograms for oil produced from 3/4" core pyrolysis. The second chromatogram shown (red) is with the internal standard containing alkanes from C14-C18.

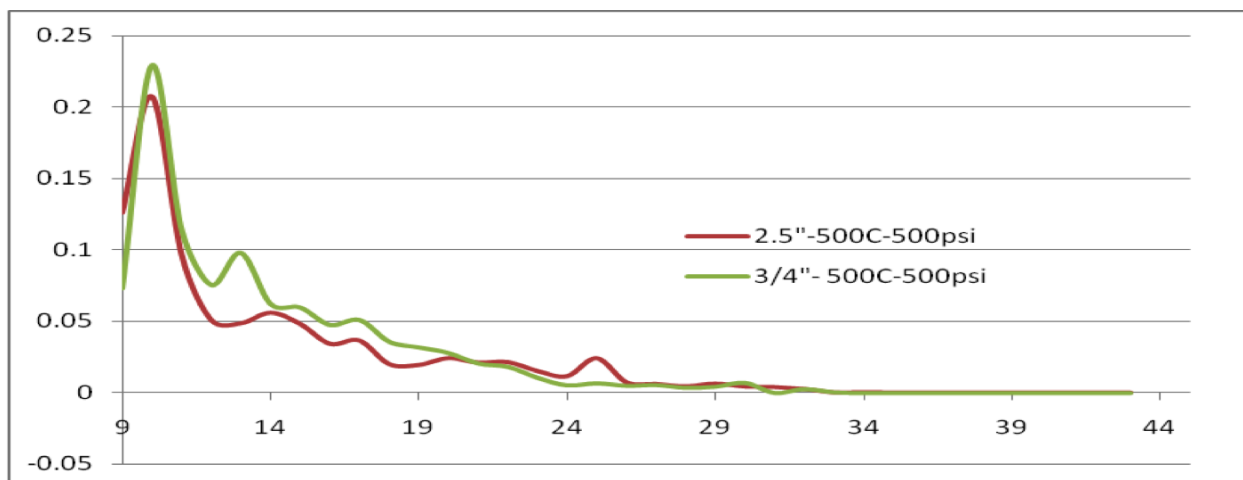


Figure 19: SCN distributions of the chromatograms obtained for oils at two different pyrolysis scales. X axis is carbon number and y axis is fraction of SCN.

Gas analysis- The gas samples collected were analyzed using a GC, which was equipped with a Pona column and with TCD and FID detectors in series. The chromatograms obtained for gaseous products are shown in Figure 20 for the 2.5" core pyrolysis and in Figure 21 for ¾" core pyrolysis. The TCD detects inorganic gases and light hydrocarbons while FID provides the responses for hydrocarbon compounds in the sample. These chromatograms show that hydrocarbons were the main constituents of the gas and that the larger sample produced relatively larger amount of lighter products. The presence of the heavier compounds in the samples depends on the condenser capacity/performance.

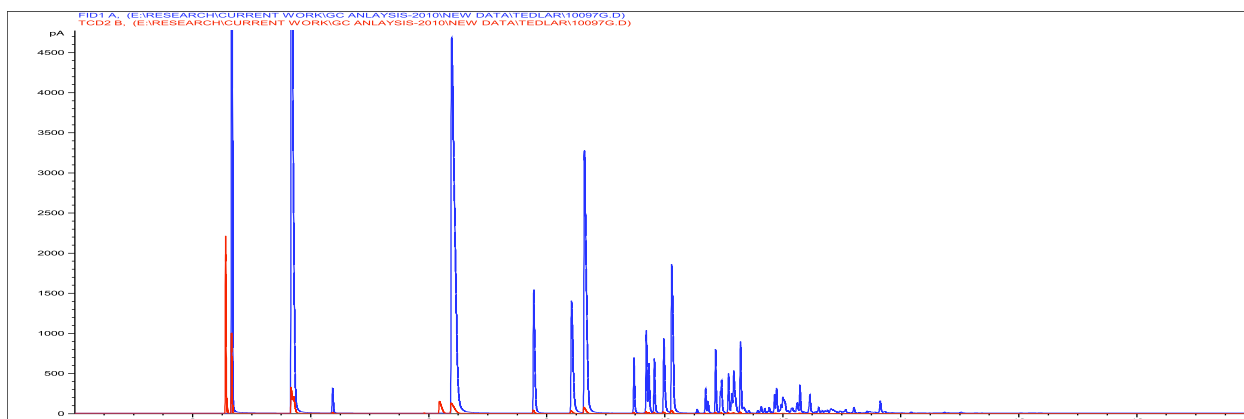


Figure 20: Chromatogram for gaseous products collected during 2.5" core pyrolysis. The two different detector responses, TCD (red) and FID (Blue) are superimposed.

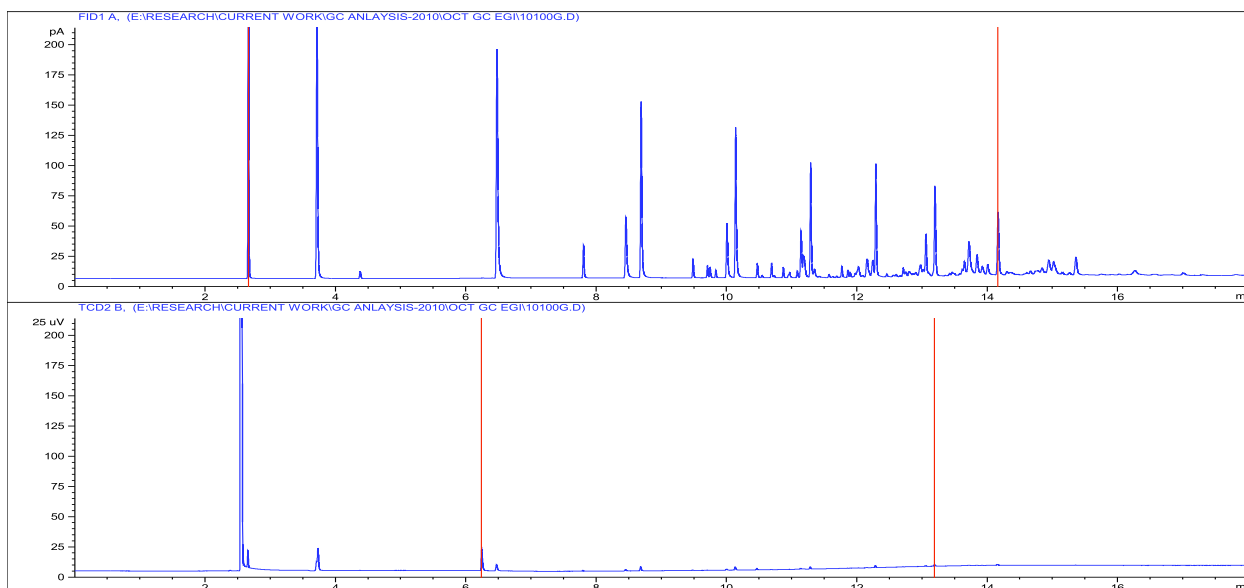


Figure 21: Chromatogram for gaseous products collected during 3/4" core pyrolysis. The two detector responses, FID (upper) and TCD (lower), are shown.

Physical properties of oil products- Densities and wax appearance temperatures for the oils obtained at the two different scales are shown in Tables 2 and 3. Within the margin of measurement, the API gravities of the two samples were identical with a small difference in the wax appearance temperature.

Table 2. Density measurement of oil using densitometer.

Samples	Density(g/cc)	API
2.5" 500C 500Psi	0.899	26
3/4" 500C 500Psi	0.898	26

Table 3. Wax appearance temperature of oil using FTIR.

Samples	WAT (Celsius)	Instrument
2.5" 500C 500Psi	19	FTIR
3/4" 500C 500Psi	17	FTIR

Spent shale analysis- The spent shales (Figure 22) were further analyzed to account for the unreacted organic and for the amount of coke formed. More fractures were seen in the 2.5" core spent shale. TGA analysis on the spent shales for the estimation of unreacted organic and coke are shown in Figure 23 and the results are included in Table 1.



Figure 22: Images of the spent shales from two different scales pyrolysis. Sample on left is 2.5” core, sample on right is 3/4” core.

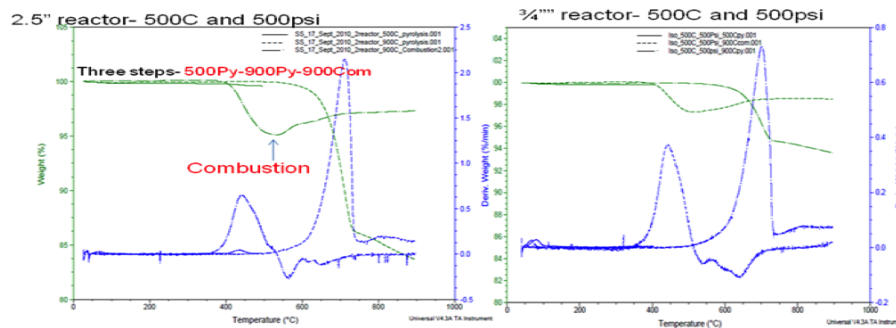


Figure 23: TGA thermograms for spent shale. Three stage process is used to estimate the unreacted organic, minerals and coke amount respectively.

Experiments Under Stress- The next step in the pyrolysis process is to perform the same type of experiments under stress. In this quarter, an apparatus was designed for this purpose. The idea is to house a core sample 2” in diameter and 20” long. The movement of the piston at the top would be calibrated to impart the right amount of in-situ stress during pyrolysis. The pressure chamber would control the pore pressure in the system. The chamber would be electrically heated with a thermocouple controlling the temperature. The chamber would be mounted in a flange/bolt assembly. These drawings, shown in Figures 24 and 25, have been provided to Professor John McLennan, under whose guidance the complete assembly will be built in the next phase of the project.

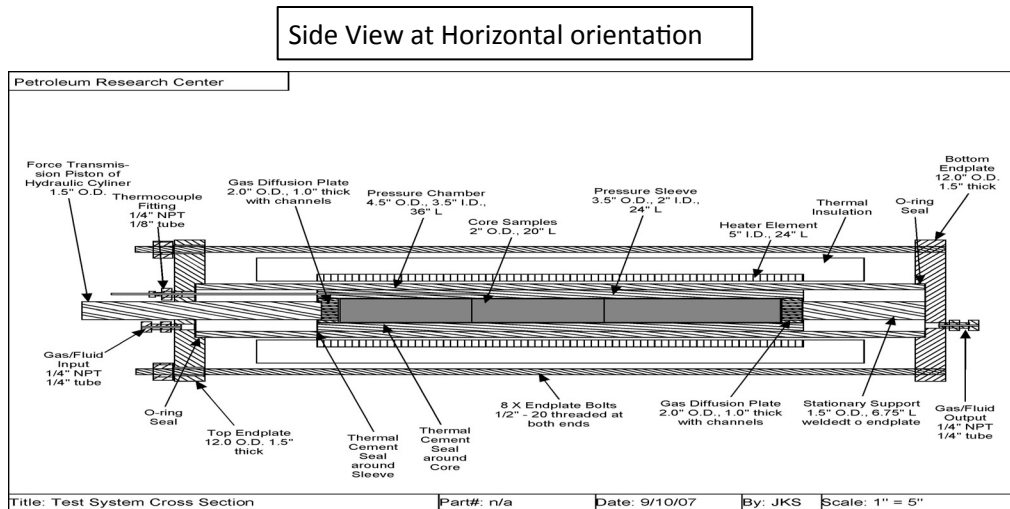


Figure 24: Detailed engineering drawing showing horizontal side view of test apparatus.

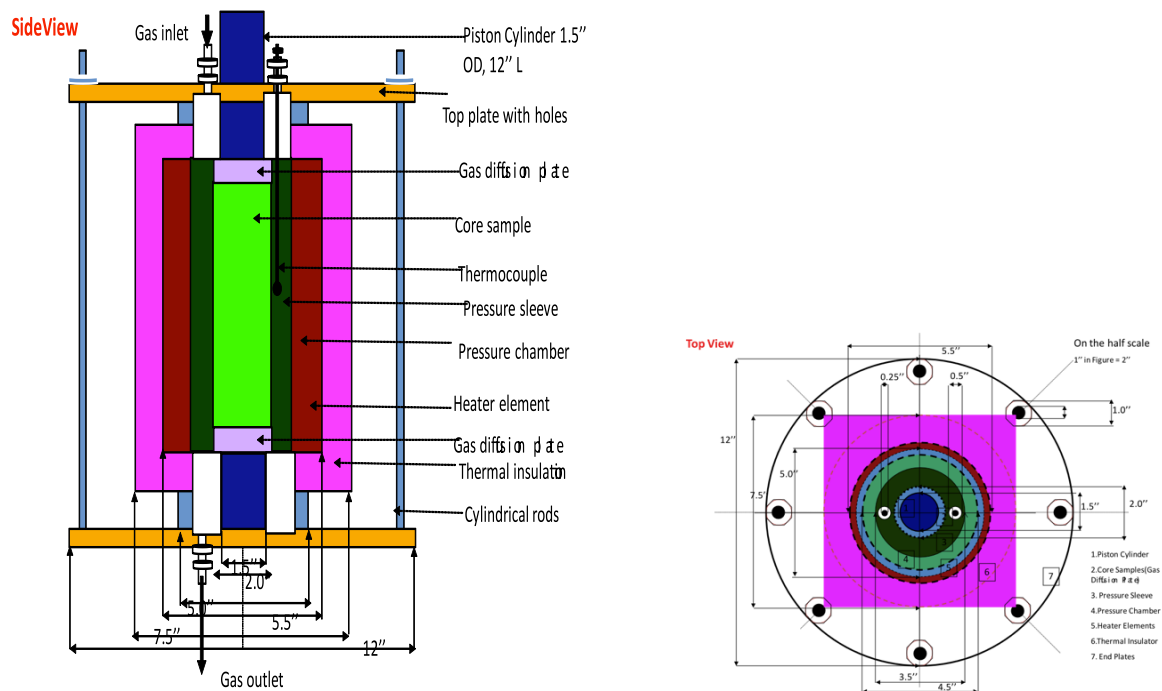


Figure 25: Schematic diagram of the induced stress measurement test apparatus; side view is on left, top view is on right.

Subtask 4.4 - Effect of Oil Shale Processing on Water Compositions (PI: Milind Deo)

When water is associated with the organic matter in oil shale, the pyrolysis process has the potential of producing water. The purpose of this project is to determine the types and concentrations of organics that may end up in the produced water. There is little water associated with the core samples from the Mahogany zone of the Green River Formation.

Hence, pyrolysis of a large core sample (2.5" in diameter) was required to produce a sufficient amount of water for analysis. Researchers in Subtask 4.4 completed the milestone to perform a preliminary analysis of process water, including some tables of aqueous phase organic species concentrations, as described below.

A 2.5" core sample (494 grams initial weight) was pyrolyzed at 350°C and at ambient pressure. Water was produced during the initial period and quickly settled. Oil production continued after the initial phase. Water and oil collected during this experiment are shown in Figure 26. The water phase was carefully separated from the oil using a pipette and further analyzed. The targets of most analyses were dissolved aliphatic, aromatic and poly-aromatic hydrocarbons.

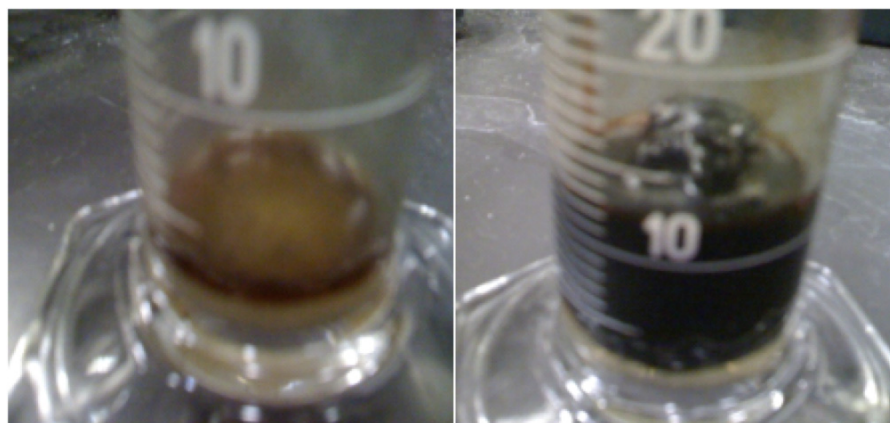


Figure 26: Left panel shows water collected during the initial phase of the pyrolysis experiment at 350°C. Right panel shows separated water-oil phases.

The following analyses were performed by American West Analytical Laboratory located in Salt Lake City, Utah.

1. Total organic carbon (TOC) in the water sample - A5310B.
2. Oil and grease (OnG) in the water sample - Method E1664A.
3. Volatile organic in the water using Gas Chromatography/Mass Spectrometry (GCMS) - Method SW-846 8260C/5030C.
4. Semi volatile organic in water using GCMS - Method SW-846 8270D/3510C

To perform the above analyses on the water phase sample, different laboratory grade surrogates were used.

The TOC and OnG results are shown in Table 4. It should be noted that the TOC is rather high – 15,000 ppm. Determination of the makeup of this organic carbon was found to be challenging, however.

Table 4. Analytical results for TOC and OnG.

Analysis	Units	Test Limit	Measured Values
Total Organic Carbon	mg/L	1000	15,500
Oil and Grease	mg/L	3000	3,070

Volatile and semi-volatile compounds were analyzed using GCMS. Results for volatile hydrocarbons are shown in Table 5. All of the compounds were below detection limits, indicating that even though the water sample contains some organics, specific species could not be identified.

Table 5. Hydrocarbons targeted by the GCMS method.

Analytical Results		VOAs Fractionation by GC/MS Method 8260C/5030C		
Analyzed: 1/7/2011 1619h				
Units: µg/L				
Dilution Factor: 1000				
Compound	CAS Number	Reporting Limit	Analytical Result	Qual
Benzene	71-43-2	2,000	< 2,000	
Ethylbenzene	100-41-4	2,000	< 2,000	
Methyl tert-butyl ether	1634-04-4	2,000	< 2,000	
Naphthalene	91-20-3	2,000	< 2,000	
Toluene	108-88-3	2,000	< 2,000	
Xylenes, Total	1330-20-7	2,000	< 2,000	
C6 Aliphatic hydrocarbons		20,000	< 20,000	
C7&C8 Aliphatic hydrocarbons		20,000	< 20,000	
C9&C10 Aliphatic hydrocarbons		20,000	< 20,000	
C9&C10 Alkyl Benzenes		20,000	< 20,000	
Surr: 1,2-Dichloroethane-d4	17060-07-0	77-144	103	
Surr: 4-Bromofluorobenzene	460-00-4	80-123	111	
Surr: Dibromofluoromethane	1868-53-7	80-124	105	
Surr: Toluene-d8	2037-26-5	80-125	103	

The reporting limits were raised due to insufficient sample volume/mass to meet normal method requirements.

The total ion spectrum of compounds (TIC) seen in GCMS during the analysis of volatile compounds is shown in Figure 27. Only the surrogates and internal standard compounds are visible along with acetone and chloroform. Acetone was a contaminant due to the glassware cleaning procedure used. The source of chloroform is not clear.

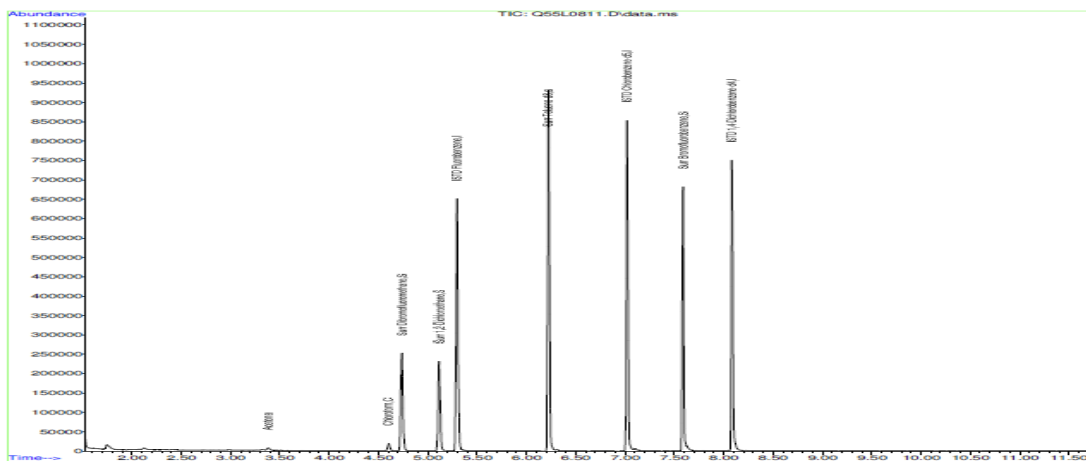


Figure 27: TIC spectrum of volatile compounds.

Results of the analysis of the semi-volatile compounds are shown in Table 6 and Figure 28. Once again, all of the targeted compounds were below detection limits. Most of the identified peaks in Figure 28 are surrogates or internal standard compounds. There are a number of unresolved peaks, however. Based on matches with compounds in the library, the compounds identified are listed in Table 7. The possible compounds are oxygen-containing aromatic compounds – phenols, organic alcohols, etc.

Table 6. Results of the analysis of semi-volatile hydrocarbons in produced water.

Analytical Results		SVOA Fractionation by GC/MS Method 8270D/3510C		
Analyzed: 1/14/2011 2200h		Extracted: 1/11/2011 1023h		
Units: µg/L				
Dilution Factor: 1				
Compound	CAS Number	Reporting Limit	Analytical Result	Qual
Acenaphthene	83-32-9	23.5	< 23.5	
Acenaphthylene	208-96-8	23.5	< 23.5	
Anthracene	120-12-7	23.5	< 23.5	
Benz(a)anthracene	56-55-3	23.5	< 23.5	
Benzo(a)pyrene	50-32-8	23.5	< 23.5	
Benzo(b)fluoranthene	205-99-2	23.5	< 23.5	
Benzo(g,h,i)perylene	191-24-2	23.5	< 23.5	
Benzo(k)fluoranthene	207-08-9	23.5	< 23.5	
Chrysene	218-01-9	23.5	< 23.5	
Dibenz(a,h)anthracene	53-70-3	23.5	< 23.5	
Fluoranthene	206-44-0	23.5	< 23.5	
Fluorene	86-73-7	23.5	< 23.5	
Indeno(1,2,3-cd)pyrene	193-39-5	23.5	< 23.5	
Phenanthrene	85-01-8	23.5	< 23.5	
Pyrene	129-00-0	23.5	< 23.5	
C11-C12 Aliphatic hydrocarbons		23.5	< 23.5	
C13-C16 Aliphatic hydrocarbons		23.5	< 23.5	
C17-C21 Aliphatic hydrocarbons		23.5	< 23.5	
C22-C35 Aliphatic hydrocarbons		23.5	< 23.5	
C11-C13 Alkyl Naphthalenes		23.5	< 23.5	
Total C12-C22 PAH**		23.5	< 23.5	
Surr: Terphenyl-d14	1718-51-0	10-199	104	

** - This value is a summation of the PAH compounds listed above.

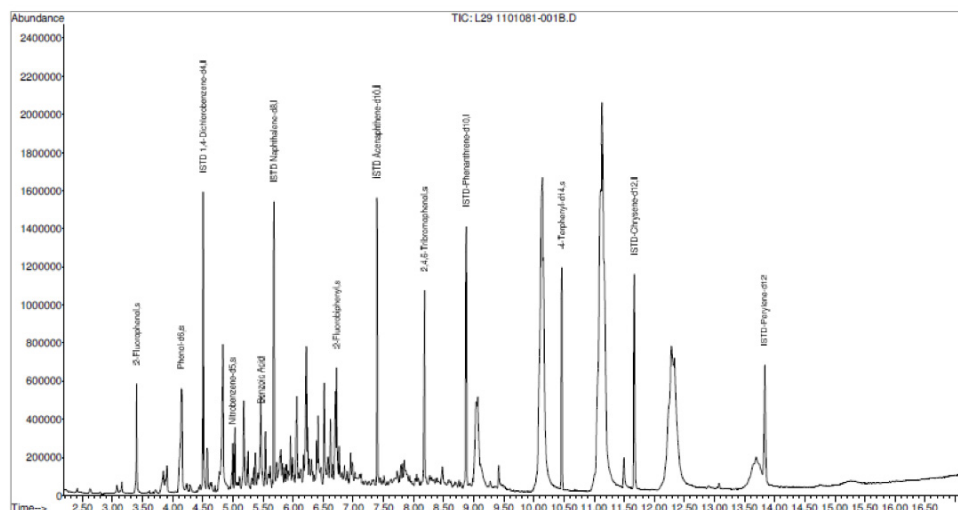


Figure 28: TIC of semi-volatile compounds.

Table 7. Possible identifications for peaks in the TIC of semi-volatile compounds.

TIC top hit name	RT	Est Conc, ug/l
Heptonic acid	4.84	36
3,4-Dimethyl-3 py..	6.06	18.8
1H-Pyrrole-2,5-di..	6.22	29
Resorcinol	6.52	19
2-Zpetanol, 1-[1-.....	9.02	26
3-Pentanol, 2-met...	10.14	214.6
3-Pentanol, 2 met...	11.11	150.7
Butanamide, 3-met...	11.13	219.2
Pentane, 2-methoxy-	12.28	115.2
2-Propanol, 1-2-...)	13.65	21.4

In summary, water produced by pyrolyzing oil shale at 350°C was analyzed in detail. The TOC was about 15,500 mg/L. The oil and grease concentration was about 3000 mg/L. There were no easily identifiable peaks in either the volatile or semi-volatile hydrocarbon categories. A list of possible compounds in the semi-volatile fraction was compiled.

Subtask 4.5 - Pore Scale Analysis of Oil Shale/Sands Pyrolysis (PI: Jan Miller, Chen-Luh Lin)

Subtask 4.5 researchers completed two milestones during this quarter. The first was to model pore network structure at different heating rates to determine porosity changes has been delayed by the lack of available samples. The second was to use multiphase LB model to analyze fluid penetration into porous samples and to provide transport information such as connectivity, conductivity, and permeability.

Porosity changes with heating rate- As reported in the previous quarter, porosity changes were determined using a 15 cm long core of indicated diameter loaded in the pyrolysis reactor. The core was heated from the outside using a band heater. A specified heating rate was used to get to the desired reaction temperature, where the core was held for 24 hours. The condensate was

collected in a series of two condensers held at -6°C . The core was cooled to ambient temperature, removed from the reactor and was subjected to high resolution X-ray microtomography (HRXMT) analysis. Results from a heating rate of $100^{\circ}\text{C}/\text{min}$ were reported last quarter. This quarter, two 1" Mahogany oil shale drill cores were pyrolyzed at two additional heating rates: MD-11 at $1^{\circ}\text{C}/\text{min}$ and MD-12 at $10^{\circ}\text{C}/\text{min}$. MD-12 had a drill hole at the center of the core for thermocouple wire.

Figure 29 shows the photos of the reaction cores at different heating rates used for the HRXMT analysis (sample from $100^{\circ}\text{C}/\text{min}$ is shown for comparison). The field of view (FOV) region is about 5 mm^3 inside the center of the reaction core for the $1^{\circ}\text{C}/\text{min}$ sample. For the $10^{\circ}\text{C}/\text{min}$ sample, the FOV is focused on the wall region between the central drill hole and the edge of the core.

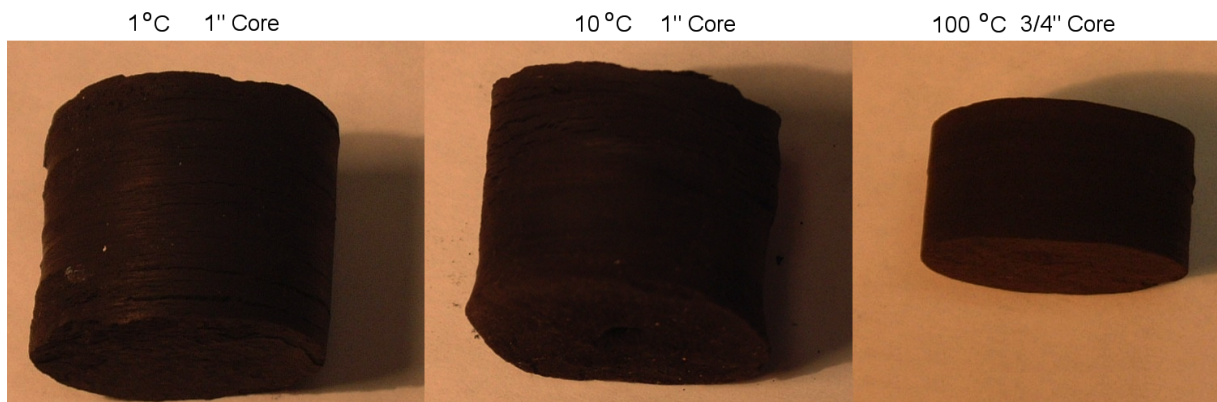


Figure 29: Reaction cores at different heating rates (1, 10 and $100^{\circ}\text{C}/\text{min}$) used for HRXMT analysis.

The 3D volume rendered images from the reconstructed X-ray computed tomography (CT) data for the Mahogany oil shale drill core samples after pyrolysis at different heating rates are shown in Figure 30. The gray scale level indicates variations in the X-ray attenuation coefficients which depend on the density and atomic number of material within each voxel. Crack networks, developed during the pyrolysis process, are evident and can be well defined. Two distinct regions with different sizes of cracks and voids are identified: the dark region shows the void space (cracks and pores) and the residual kerogen while the light region shows the layers of mineral matter (clay and carbonates).

Porosity, the simplest property of such porous structures, is defined as the volume fraction of pores. Porosity can be used to predict the permeability defined by Darcy's law. The porosity of oil shale after pyrolysis can be used to predict the permeability for pore-scale network modeling or from Lattice-Boltzman simulations as reported previously. Quantitative information on porosity change of oil shale samples after pyrolysis can be determined from the CT data.

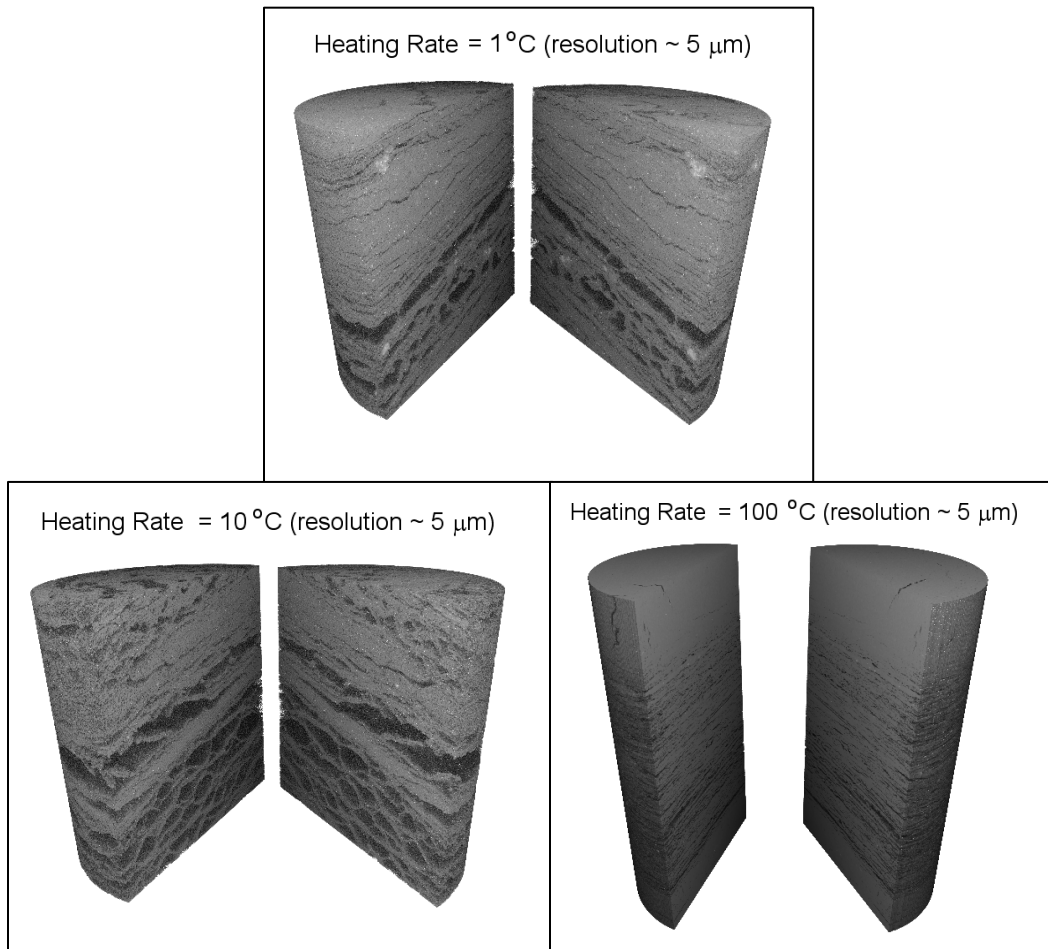


Figure 30: Volume rendered images of Mahogany oil shale drill core samples after pyrolysis at different heating rates (1, 10 and 100°C/min). Images are from the reconstructions of HRXMT data at ~5 μm voxel resolution.

Figures 31 and 32 illustrate the overall views of the 1" oil shale drill core samples after pyrolysis at heating rates of 1 and 10°C/min, respectively, and the corresponding porosity profiles measured from the CT data along the height of the drill core samples. The porosity is defined as the ratio between the void area and the total area of each cross section. As expected, higher porosities are obtained for the kerogen-rich layer of the pyrolyzed oil shale drill core samples. The mean porosity change of the silicate-rich layers inside the reacted core is about 10% for the heating rates of 1 and 100°C/min. However, results from the 10°C/min heating rate indicate higher mean porosity for the silicate-rich layers. It seems that the drill hole at the center of the core influenced the crack formation for the silicate rich layers and the mean porosity is increased from about 10% to 20%. It should be noted that the reported porosity may be overestimated since residual kerogen and kerogen reaction products may be included.

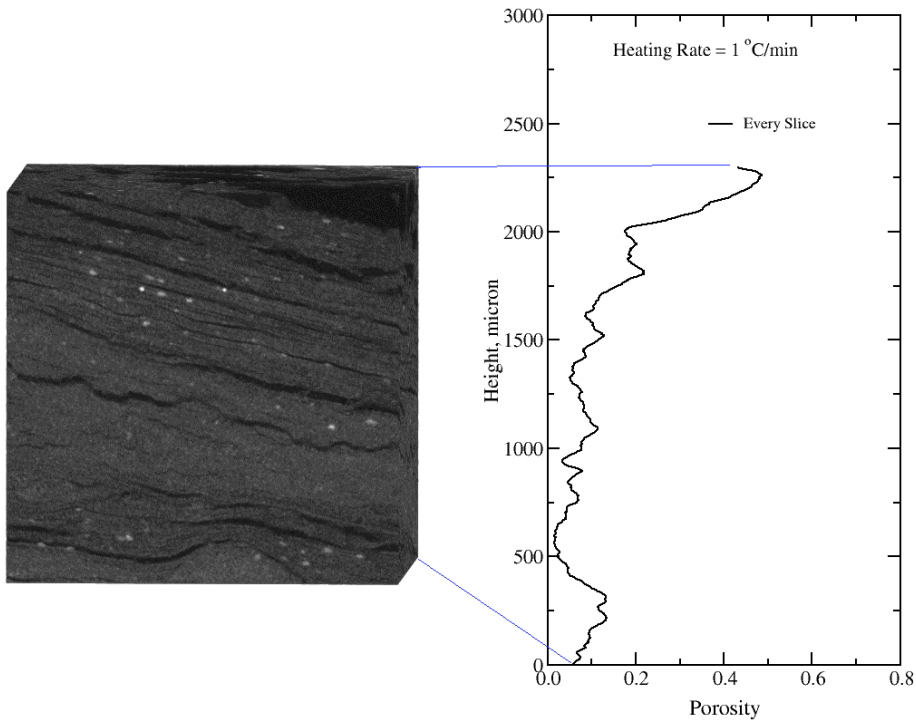


Figure 31: Overall view of Mahogany oil shale drill core samples after pyrolysis at $1^{\circ}\text{C}/\text{min}$ heating rate. Cracks are identified by the black region of sample images on the left. The porosity variation with drill core sample height as measured from the CT data is shown on the right.

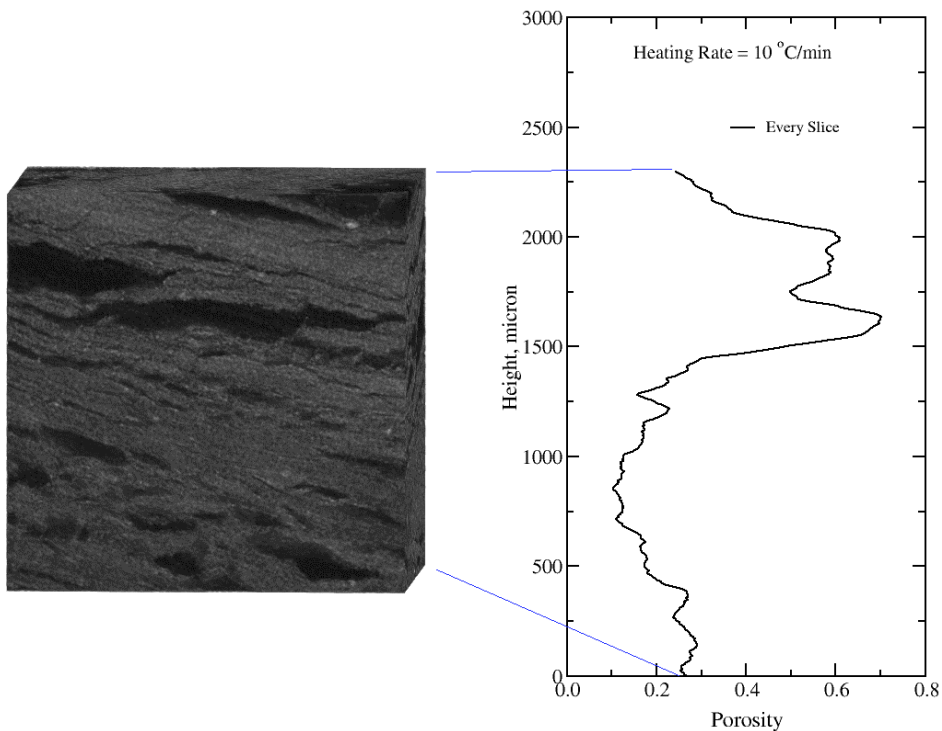


Figure 32: Overall view of Mahogany oil shale drill core sample after pyrolysis at $10^{\circ}\text{C}/\text{min}$ heating rate. Cracks are identified by the black region of sample images on the left. The porosity variation with drill core sample height as measured from the CT data is shown on the right.

Multiphase LB model simulation of fluid transport- The flow of two immiscible fluids sharing simultaneously the complex pore space in a porous medium is governed by the forces acting on the fluids: pressure, viscous, gravitational, inertial and interfacial surface. The relative importance of each of these forces is usually characterized by the Reynolds (Re), Bond (Bo), and Capillary (Ca) numbers, as well as the viscosity ratio (M). These parameters are defined in equations 1 through 4, respectively.

$$Re = \frac{u \times D}{\nu} \quad (1)$$

$$Bo = \frac{g(\rho_{nw} - \rho_w) \times R^2}{\gamma} \quad (2)$$

$$Ca = \frac{\nu_w u_w}{\gamma} \quad (3)$$

$$M = \frac{\mu_{nw}}{\mu_w} \quad (4)$$

Because pressure forces and viscous forces are proportional to the rate of flow, these forces are less important with a slow flow rate. Also, inertial forces are negligible. Hence, the capillary and gravitational forces become more important when the rate of flow is slower.

Capillary pressure- When two immiscible fluids are in contact in the porous medium, a discontinuity in pressure exists across the interface. This pressure difference is called the capillary pressure. Capillary pressure is defined as the difference between the pressures of the non-wetting fluid and the wetting fluid. Figure 33 shows a curved interface between two immiscible fluids under static equilibrium. From the figure it is observed that capillary pressure depends in the curvature of the interface.

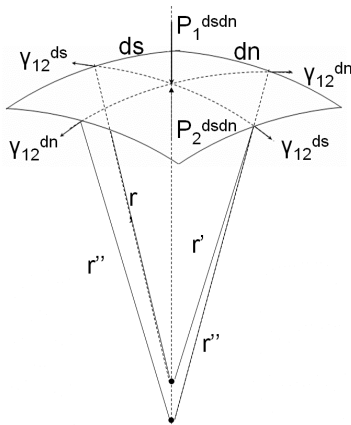


Figure 33: Forces acting on the elementary surface around a point of a curved interface between two immiscible fluids at static equilibrium.

Interfacial shapes in static and quasi-static situations are governed by the Laplace equation. By applying the condition of mechanical equilibrium of the forces acting on the interface, Laplace showed that the capillary pressure is proportional to the interfacial tension and inversely proportional to the curvature of the meniscus.

Interfacial tension and contact angle- Porous structures involve the presence of a solid phase which in a capillary system interacts with at least two fluid phases. As a result, there are at least three surfaces subjected to surface tension as shown in Figure 34. The static equilibrium between the three interfacial tensions leads to Young's equation as shown in equation 5.

$$\gamma_{lg} \cos\theta = \gamma_{sg} - \gamma_{sl} \quad (5)$$

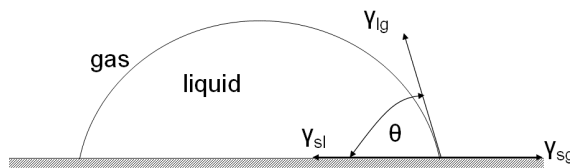


Figure 34: Static equilibrium between the three interfacial tensions at the solid surface.

The contact angle is normally used to describe the preferential characteristics of the solid surface to be wet. In some cases, no equilibrium is possible and the liquid covers the whole surface completely. In such cases, the liquid is said to wet the solid perfectly.

Capillary pressure versus saturation curves- The capillary pressure depends on the saturation, interfacial tension, wetting angle, viscosity ratio and Bond number (Marle, 1981). Because the capillary pressure depends on the contact angle, different capillary pressure–saturation curves are obtained depending on the history of the fluid motion, e.g. whether a sample was initially saturated with the wetting or non-wetting fluid component. If the sample is initially saturated with the wetting fluid, an increment of the capillary pressure produces the displacement of the wetting fluid for the non-wetting fluid in a process known as drainage. If the sample is initially saturated with the non-wetting fluid, a decrease in the capillary pressure produces imbibition. Figure 35 shows a typical curve revealing the relation of capillary pressure to saturation. The entry point P^* shows that if a sample is initially saturated by a wetting fluid, a certain pressure (threshold pressure or non-wetting entry value) must be built up before the non-wetting fluid begins to penetrate the sample. The figure also shows that at high capillary pressure, the

wetting saturation reaches a minimum limit, S_{w0} . The imbibition curve shows that a maximum limiting saturation value is reached at zero capillary pressure. This point corresponds to the

residual saturation S_{mnv0} of non-wetting fluids that stay entrapped in the porous solid. It is well known that pressure–saturation curves are subject to hysteresis phenomena and therefore the capillary pressure is a function of the direction of displacement and the history of the two-phase flow in the porous sample.

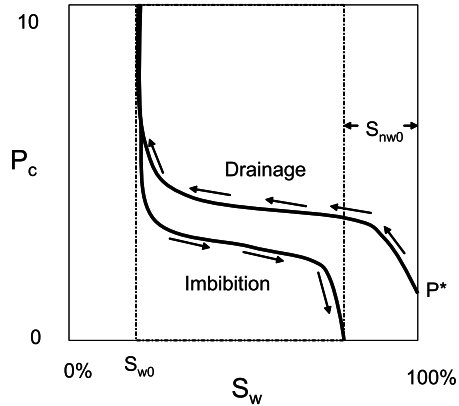


Figure 35: Typical capillary pressure curve.

Single component multiphase He-Chen-Zhang model- In order to describe fluid motion, a multiphase Lattice-Boltzmann fluid flow model (LBM) is required to investigate the flow through the porous media. The major advantage claimed for pursuing the use of LBM instead of standard CFD methods resides in its ability to model complex solid boundaries in any arbitrary geometry and to incorporate microscopic force interactions that control the interface dynamics.

In general, the LBMs for multiphase flow can be described as single component or multicomponent models. Single component models describe phase separation by an equation of state that, under the critical temperature, automatically segregates phases into two stable densities, vapor and liquid. Multicomponent models use one particle distribution function (PDF) and one evolution equation to represent each fluid component in the system and segregation is simulated by interaction between the two independent fluids.

Subtask 4.5 researchers started with the description of the single-component multiphase flow developed by He, Chen and Zhang (1999). The He-Chen-Zhang model simulates the interfacial dynamics, e.g. phase segregation and surface tension, from mesoscopic kinetic equations. In this model, the interfacial dynamics are the result of molecular interactions where two distributions functions are used, one for tracking the pressure and velocity and another for tracking the density. When the molecular attraction is strong enough, the fluid automatically segregates into two different phases.

Simulation of fluid penetration and capillary phenomena in porous media- The solid-fluid interaction explained before can be extended to the analysis and simulation of two-phase flow in complex porous structures. First, the behavior of the LB model in simple capillary tubes is illustrated, then the model is expanded for the simulation of fluid penetration in an actual 3D image of oil sand as obtained from XMT analysis.

In a capillary tube, there is fluid displacement when the flow is driven by a difference in pressure strong enough to overcome the capillary pressure. Figure 36 shows LB simulated results for capillary tubes where the non-wetting fluid displaces the wetting fluid from left to right for several driving pressure differences. From these images, it is possible to observe that the wettability of the wall creates a wetting film at the surface which remains attached to the wall while the non-wetting fluid front advances. The width of this wetting film depends of the strength of the attraction and herein the result is about three lattice units.

In LBM simulations, the difference in pressure between the inlet and outlet can be set by fixing the density of the fluids where the densities are related to the pressure by the equation of state. The entry pressure for displacement of one fluid by another in a porous capillary is a function of the radius of the pore, the surface tension of the fluids, and the contact angle.

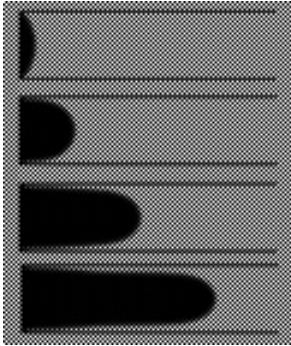


Figure 36: Simulations of fluid displacement for increasing difference in pressure. Values from top to bottom: 0.2508, 0.2498, 0.2482 and 0.2466. D2Q9 lattice of size 35x130 lu².

The capillary phenomenon of interest, similar to the network microstructure of oil sands/oil shale, is the behavior of the system when two or more capillary tubes (throats) are present. Figure 37 shows the simplest case of two-phase flow of two porous channels of different diameters under the same pressure difference. One of the throats is six times smaller than the other and therefore has a six times higher entry pressure. The pressure across the phases has been set in such a way that the value is higher than the entry pressure for the bigger diameter throat but smaller than the entry pressure for the smaller diameter throat. Figure 37 shows a sequence of images from left to right and top to bottom where it is possible to observe the preferential flow that is developed by the meniscus which invades the channel with the higher throat radius having a smaller flow resistance.

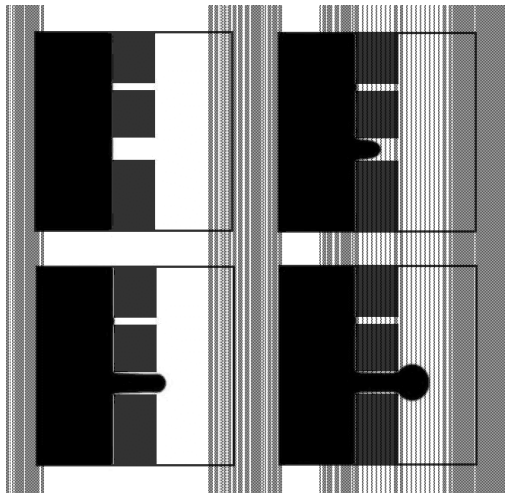


Figure 37: Simulations of fluid displacement in a capillary tube with two throats of different radius. From left to right and top to bottom: flow after 1000, 10000, 20000 and 30000 iterations. D2Q9 lattice of size 35x130 lu².

From these results, it is evident that this modified He-Chen-Zhang model has good qualitative agreement with theory for two-phase flow in porous media. Hence, Subtask 4.5 researchers proceeded with application to actual porous network structures such as those found in the pyrolysis of oil sands/oil shale.

Lenormand et al (1988) proposed a phase diagram for immiscible displacement characterized by the capillary number (eq. 3) and the viscosity ratio (eq. 4) as shown in Figure 38. The diagram shows the existence of three basic domains for fluid penetration: stable displacement, viscous fingering, and capillary fingering. In the stable displacement region, the major force is due to viscosity interaction of the injected fluid. The flow shows a flat front moving towards the exit with some irregularities with the dimensions of a few pore scales. In the viscous fingering region, the major force is due to viscosity interaction of the displaced fluid. The fingers look like a tree with no loops. They spread across the porous network, growing towards the exit. In the capillary fingering region, the major force is due to capillarity, which also exhibits tree-like fingering, but the fingers grow in all directions forming loops. These loops trap the displaced wetting fluid leading to a higher final saturation than the viscous fingering.

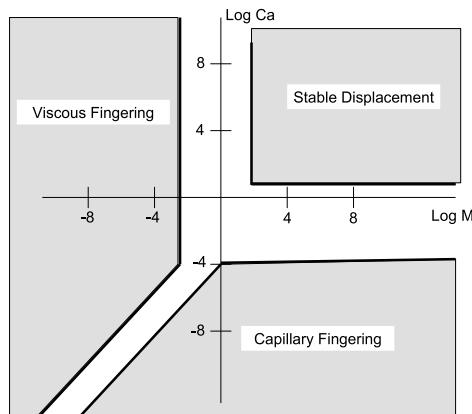


Figure 38: Lenormand Diagram (after Lenormand et al, 1988)

Figure 39 shows 2D simulations of the interface advance using the single component He-Chen-Zhang LBM applied to a packed bed of sand particles where the pore network structure has been captured by XMT analysis. In this simulation, a two-dimensional XMT image slice has been used and flow goes from top to bottom, induced by a fixed pressure difference. Parameters of the simulation are set in such a way as to obtain flow in the transition zone between capillary fingering and stable displacement. The capillary number is 6.77×10^{-2} and the density ratio is 3.

As can be seen in the sequence of images, the simulation starts from complete saturation of the wetting phase. In the course of simulation, the flow follows less resistant paths (coarser pore diameters), leaving behind some residual wetting phase trapped in very small pore spaces where the non-wetting phase cannot enter until the pressure increases. In agreement with the diagram proposed by Lenormand et al (1988), the pattern of percolation shows a capillary fingering type of flow with relatively short fingers.

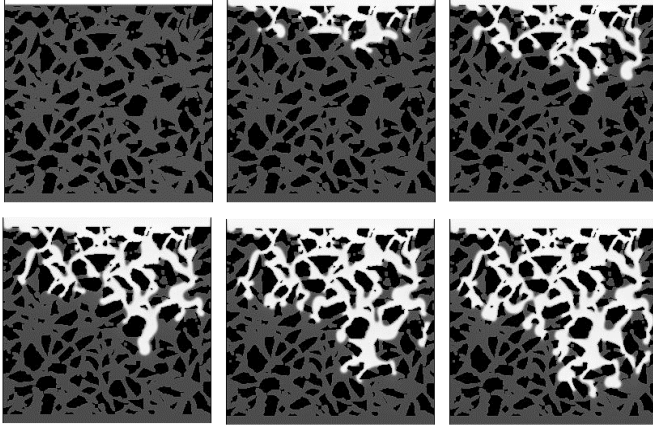


Figure 39: Sequence of simulations of two-phase flow in a packed bed of sand particles. Lattice size of 256x256. Images show each 5000 iteration steps.

Figure 40 shows a comparison of the same structure shown in Figure 39 with a 2D simulation condition where the surface tension is varied. A comparison at the same level of iteration shows that the percolation follows the same pattern for both multiphase flows in this porous network structure, probably due to the fact that both simulations are run with the same pressure gradient and therefore the path of least resistance has not changed. However, reduction of the surface tension produces longer and thinner fingers.

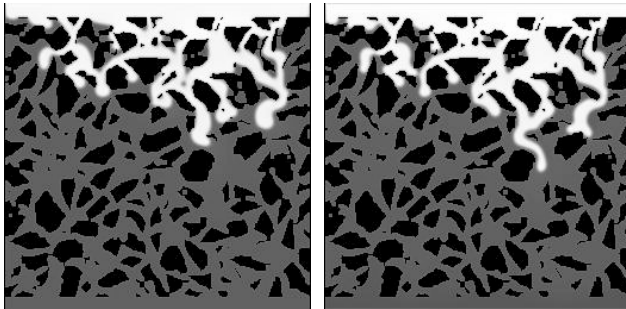


Figure 40: Penetration simulations for two different surface tensions after 10,000 iterations. Left image has a high surface tension ($\bar{k}=0.1$, $Ca = 6.77 \times 10^{-2}$) and right image has a low surface tension ($\bar{k}=10^{-5}$, $Ca = 230$).

Figure 41 shows a comparison between the 2D simulations of Figure 39 (left image) with a simulation where the density ratio has been inverted (right image). In this new case, the low density fluid displaces the heavier fluid and the pattern of flow changes since the pressure field has changed. According to the Lenormand diagram (Figure 38), a stronger viscous fingering type of flow is expected with more and longer fingers being formed due to the stronger viscous interaction and interface front instability. As the comparison shows, there is a clear qualitative agreement between theory and simulations. Fingers are formed in zones of low resistance to flow and once formed they start growing rapidly towards the exit.

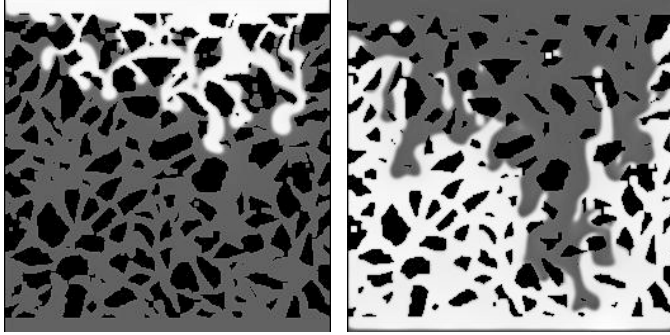


Figure 41: Two different penetration simulations after 10,000 iterations for the same surface tension but inverse density ratio. Left image has a density ratio =3/1 and $Ca = 6.77 \times 10^{-2}$. Right image has a density ratio =1/3 and $Ca = 1.32 \times 10^{-1}$.

The single component multiphase flow He-Chen-Zhang LBM model has been extended to incorporate fluid-solid interaction forces and has been applied to the simulation of percolation in actual XMT images of pore network structures for the Athabasca (Alberta) and Sunnyside (Utah) oil sand samples. Results from LBM simulations for oil sands samples from Athabasca, Alberta and from Sunnyside, Utah are shown in Figures 42 and 43 respectively. A more uniform pore network structure (e.g. stable displacement of the front) was observed due to the narrow size distribution of the sands from the Athabasca sample. A more complex pore network structure was observed (e.g. capillary fingering) for the Sunnyside oil sand sample due to the wide spread of the sand size distribution.

Athabasca Oil Sand (2.0x2.0x1.6 mm)

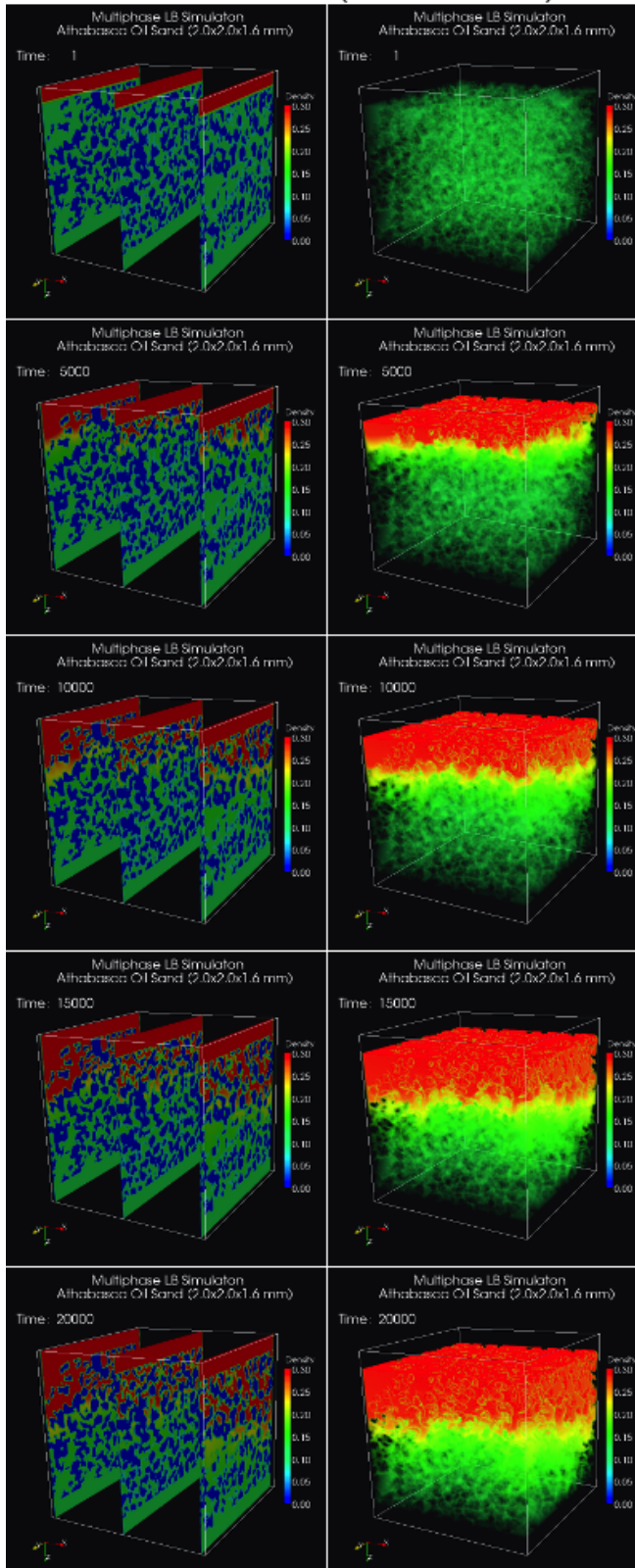


Figure 42: Results of LB simulation of multiphase flow through Athabasca oil sand sample. Top to bottom image: flow after 1, 5000, 10000, 15000 and 20000 iterations.

Sunnyside Oil Sand (2.0x2.0x1.6 mm)

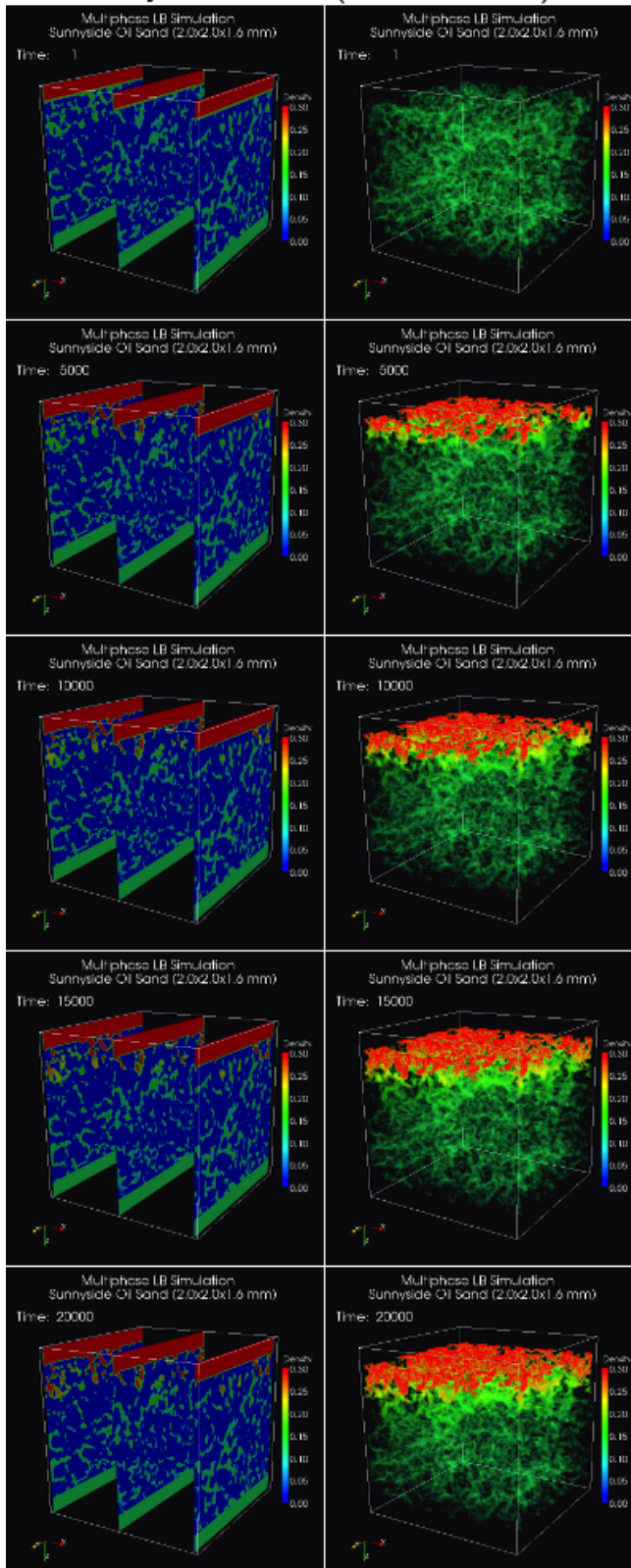


Figure 43: Results of LB simulation of multiphase flow through Sunnyside oil sand sample. Top to bottom image: flow after 1, 5000, 10000, 15000 and 20000 iterations.

Subtask 4.6 - Kerogen/Asphaltene/Mineral Matrix: Structure and Interactions (PI: Julio Facelli, Ronald Pugmire)

This quarter, the Project Team's milestone was to "correlate analytical spectroscopic data of isolated and absorbed 3D models and establish its sensitivity to model structural features." This milestone was accomplished in this reporting period by calculating both NMR and IR data on the six asphaltene models proposed by Siskin et al. (2006) as discussed in the third quarter 2010 report. Based in the results for this milestone described below, the Project Team has established that the data is sensitive to changes in the model used.

For all calculations we started with the STO-3G optimized structures reported previously. The NMR calculations were done with Gaussian09 using the PBE1PBE DFT functional and the 6-311G basis function. The resultant ^{13}C chemical shielding values were referenced to the TMS scale with the chemical shielding of CH_4 at the same level of theory and the basis set being referenced to the known gas phase chemical shift of CH_4 of -7 ppm. The calculated chemical shifts were then broadened (aliphatic with 2ppm, aromatic with 5ppm) and plotted. The plots of the spectra of all six of the asphaltenes are shown in Figure 44. The six spectra show distinct differences, indicative of the differences in the asphaltenes while also verifying that NMR is sensitive to the differing structural features of the models. In Figure 45, the calculated spectrum of the mid-continent asphaltene is compared with the experimental solid state ^{13}C spectrum; this is the only asphaltene for which the experimental ^{13}C NMR spectrum has been published. The Project Team is in contact with Dr. Kelemen (coauthor of Siskin et al. paper) to see if he can make the spectra of the other five asphaltenes available. From the analysis of the spectra presented in Siskin et al. (2006), Team members expect the six spectra to show marked differences.

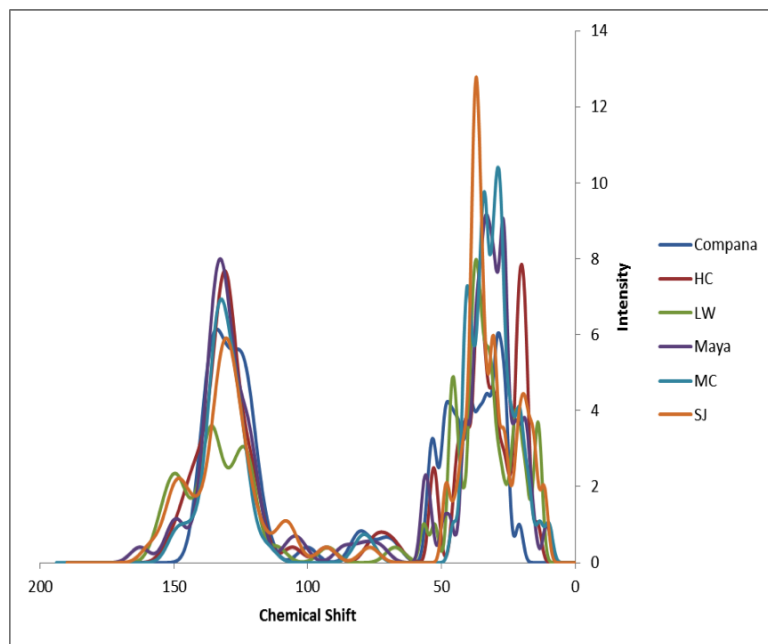


Figure 44: Comparison of calculated ^{13}C NMR for the six asphaltene models.

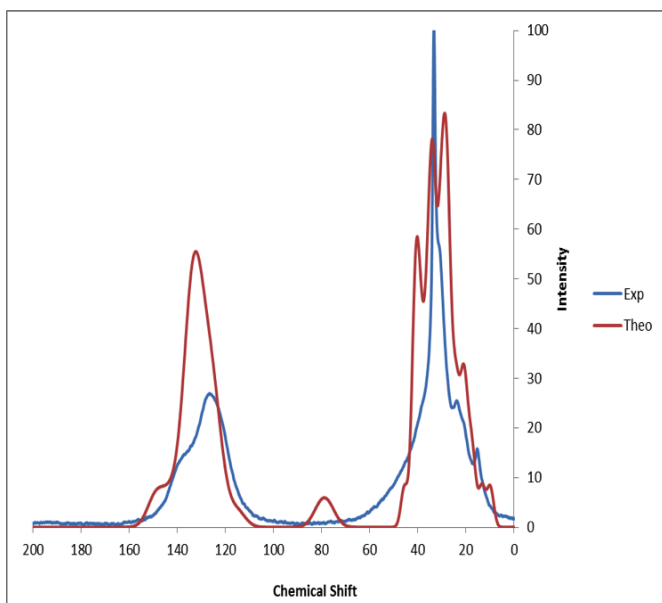


Figure 45: Comparison of calculated and experimental ^{13}C NMR of mid-continent US asphaltene.

One reason for the differences between experiment and theory is that calculations are performed on a single representative model structure, whereas the real sample is a very complex mixture. In addition, asphaltenes are known to aggregate via stacking, and intermolecular interactions can also contribute to the observed chemical shifts. Previously, Team members optimized stacks of three of the Campana asphaltenes in three different manners: parallel stacks, inverted stacks, and anti-parallel stacks at the STO-3G level. The parallel stack was determined to be the lowest energy of these three. The Project Team has taken this lowest-energy stack and completed the chemical shielding calculations. Figure 46 shows the comparison of the calculated ^{13}C NMR chemical shifts for the single Campana unit and for the parallel stack.

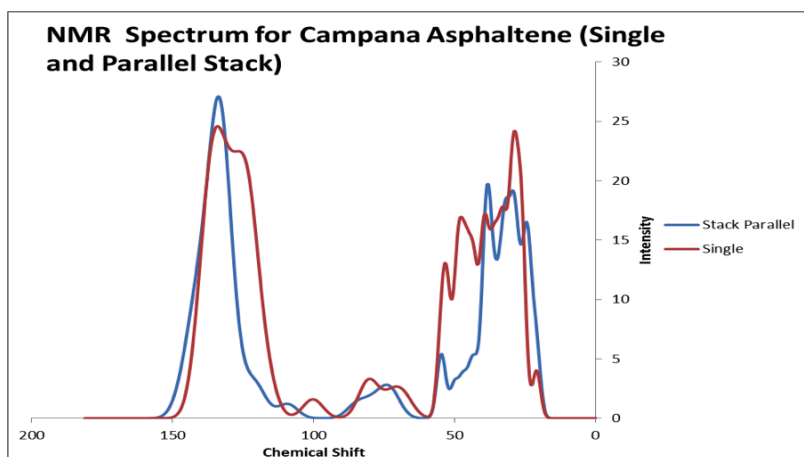


Figure 46: Comparison of calculated ^{13}C NMR of single unit and of parallel (lowest E) stack for model of Campana asphaltene.

Finally, the Project Team calculated the vibrational frequencies for the six different single molecule asphaltene models. These calculations were completed on the same STO-3G optimized structures with Gaussian09 using the same functional mentioned above but at the STO-3G basis set level. The resulting calculated IR spectra are shown in Figure 47 for two of the six asphaltenes. As can be seen from these spectra, IR is a second spectroscopic method that is sensitive to changes in the model structure.

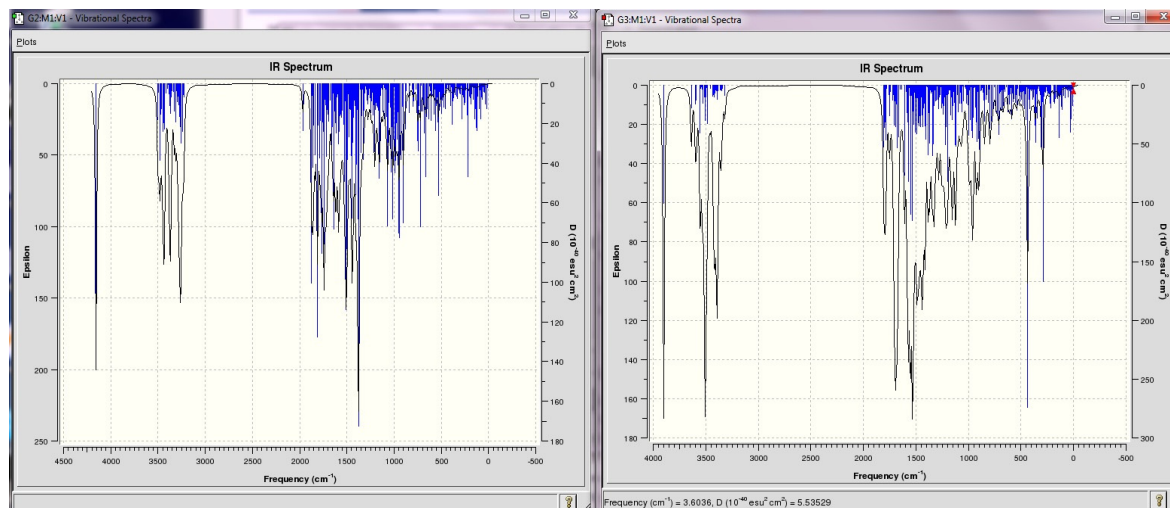


Figure 47: Calculated IR spectra of two model asphaltenes: Mid-continent US (left) and Campana (right).

The Project Team added the NMR results to the paper "Ab Initio Calculation of Asphaltenes" by Pimienta, Badu, Orendt, Facelli and Pugmire mentioned in the last quarterly report. This paper will summarize the work on the six representative asphaltene structures outlined above and in the previous two quarterly reports. The manuscript will be submitted to *Energy & Fuels*.

Team members continue to hold the manuscript entitled "Three-Dimensional Structure of the Siskin Green River Oil Shale Kerogen Model: A Computational Study" by Pimienta, Orendt, Pugmire, Facelli, Locke, Winans, Chapman and Chupas until they can get experimental atomic pairwise distribution function measurements on a kerogen sample isolated from a section of the Skyline 16 core obtained by ICSE (see report from second quarter of 2010). This experimental data will be used to evaluate the 3D kerogen structure based on the Siskin model obtained from previous computational efforts associated with this task.

Task 5.0 - Environmental, Legal, Economic and Policy Framework

Subtask 5.1 – Land and Resource Management Issues Relevant to Deploying In-situ Thermal Technologies (PI: Robert Keiter, John Ruple)

During the fourth quarter of 2010, Subtask 5.1 researchers focused on pending oil and gas development projects potentially conflicting with oil shale and oil sands development, Indian Country jurisdiction, finalizing oil shale and oil sands mapping and quantification, and finalizing the Land Use Topical Report. Researchers met with or discussed report topics with representatives from the Environmental Protection Agency, Utah Department of Environmental Quality, Utah Division of Oil Gas and Mining, Governor's Public Lands Office, and the National Oil Shale Association. ICSE researchers also attended the Utah Water Users Association

conference addressing proposed legislation and watershed planning, and the Utah State Bar Associations Environmental & Natural Resource Law section's semi-annual meeting discussing recent legal developments in this area. A draft report was circulated to academic and industry reviewers. Comments were reviewed and integrated into the Topical Report, final layout and editing were completed, and the final report was prepared for submission to the Department of Energy – NETL.

The Journal of Land, Resources and Environmental Law agreed to publish an article prepared by Subtask 5.2 researchers on Indian Country jurisdiction and its implications for energy development within the Uinta Basin. The article will appear in the fall 2011 issue and satisfies the final deliverable for this Subtask.

Subtask 5.2 - Policy Analysis of Water Availability and Produced Water Issues Associated with In-situ Thermal Technologies (PI: Robert Keiter, John Ruple)

During this quarter, Subtask 5.2 researchers continued to research and draft sections of the Produced Water Topical Report. Researchers discussed report-related issues with representatives from the Utah Division of Water Rights, Utah Division of Water Resources, state legal counsel, private sector water lawyers, and major water purveyors. Subtask 5.2 researchers completed a rough draft of the Topical Report for distribution to reviewers from the National Oil Shale Association, Office of the Utah State Engineer, Office of the Utah Attorney General, and ICSE faculty. Reviewer comments were integrated into the Topical Report, final layout and editing were completed, and the final draft of the Topical Report was prepared for submission to the Department of Energy - NETL. Completion of the Topical Report satisfies the final deliverable for this Subtask.

6.0 – Economic and Policy Assessment of Domestic Unconventional Fuels Industry

Subtask 6.1 Engineering Process Models for Economic Impact Analysis (PI: Terry Ring)

In this quarter, Subtask 6.1 had a milestone to upload all models used and data collected to the ICSE repository. The completion of this milestone has been delayed as models for the process flow sheets and economics of heavy oil extraction are still not complete. After completed models for conventional (vertical) drilling were evaluated for economics, the supply costs were very high for all in situ extraction methods (oil shale and oil sands) and for heavy oil from Alaska. As a result, the models were reworked to consider the effect of horizontal drilling on process economics. In addition, the blending of natural gas condensates with heavy oil from Alaska was requested to lower the high cost of on-site upgrading. This approach removes the need for extensive hydrogen generation system on site. This reworking of the in situ production scenarios has only just been completed for Alaskan heavy oil but not for the in situ oil sands that use SAGD for extraction and for the in situ oil shale that uses conductive heating for extraction. Subtask 6.1 researchers are still working out the modeling details and bugs for these two extraction systems. When the models and data are complete, they will be uploaded to the repository.

Additionally, Subtask 6.2 researchers were engaged in writing drafts of sections for the Market Assessment (Subtask 6.3), completing the engineering and economic analyses for the five unconventional fuels development scenarios to be included in the Market Assessment (ex-situ oil shale, in-situ oil shale, ex-situ oil sands, in-situ oil sands, Alaskan heavy oil), and checking the various scenarios for internal and scenario-to-scenario consistency. One graduate student, Bernardo Castro, finished his MS thesis and left to pursue his PhD thesis elsewhere during the quarter. Team members have encountered some internal and scenario-to-scenario inconsistencies during the quarter and have had to slow work on writing the final report to be

assured that the data going into it is accurate. This accuracy checking must be completed before the finalized data can be reported out.

Subtask 6.2 - Policy analysis of the Canadian oil sands experience (PI: Kirsten Uchitel)

During this quarter, Subtask 6.2 researchers completed research and analysis related to taxes and royalties levied on oil sands production, as well as downstream and marketing challenges facing oil sands development. Specifically, Subtask 6.2 researchers (1) examined the economic basis of mineral taxation, including the notion of "economic rent," which has played a central role in the theory and practice of mineral taxation policy, (2) reviewed the historical and current tax and royalty policies ("fiscal system") applying to the Alberta oil sands, and (3) reviewed fiscal systems applying to conventional onshore oil production in the U.S. Researchers also completed analysis and writing of their economic research findings and applied those research findings to the issues addressed in the Oil Sands Topical Report. Researchers specifically addressed the relevance for oil sands development of two general research findings: (1) if the primary goal of mineral taxation policy is to encourage development, then the standard U.S. fiscal system applying to conventional onshore production may be a poor choice for unconventional production as the standard U.S. fiscal system is largely based on the gross revenues from extracting oil from a deposit, rather than the rent of the deposit; and (2) the low rent of unconventional resources such as oil sands and oil shale does not imply that they should be taxed delicately (e.g. according to rent) as policymakers may decide that the negative environmental or sociological side-effects are severe enough that purposeful, active discouragement of such projects is warranted.

Subtask 6.3 – Market Assessment Report (PI: Jennifer Spinti)

The focus of the Project Team during this quarter was the preparation of a draft release of the Market Assessment report. The draft version of the first five sections of the report has been completed and is available in PDF form upon request. However, the release of the draft has been delayed by economics for conventional vertical drilling that rendered all three in situ scenarios unusable. The new draft release date is April 2011 with a release date for the final report of June 2011.

CONCLUSIONS

The Clean and Secure Energy from Domestic Oil Shale and Oil Sands Resources program has circulated its External Advisory Board recommendations and is transitioning its repository to the new host, the University of Utah's Institutional Repository. Researchers in the thrust area related to oil shale and sands utilization with CO₂ management have completed a tool for estimating life-cycle GHG emissions from process models developed in Subtask 6.1 and have successfully complete initial simulations with the oxy-fired ENEL TEA-C burner. Researchers in the thrust area related to liquid fuel production from in-situ thermal treatment of oil shale/sands have published several papers related to their work in kerogen pyrolysis, reservoir simulation of in situ processes, and 3D multiphase flow simulation in porous media. In addition, a regional cross-section of oil shale deposits in the Uinta Basin has been completed and work continues with Red Leaf Resources to simulate heat transfer in their Ecoshale capsule. Researchers in the environment and policy thrust area have recently submitted two Topical Reports, one relating to land use issues in the deployment of in situ thermal technologies and the other targeting produced water. Researchers in the market assessment thrust area completed Sections 1-5 of the draft Market Assessment report and are finishing up Sections 6-10.

COST STATUS

COST PLAN/STATUS

Baseline Reporting Quarter	Yr. 1							
	Q1		Q2		Q3		Q4	
	7/1/09 - 12/31/09		1/1/10 - 3/31/10		4/1/10 - 6/30/10		7/1/10 - 9/30/10	
	Q5	Total	Q6	Total	Q7	Total	Q8	Total
Baseline Cost Plan								
Federal Share	484,728	484,728	484,728	969,456	484,728	1,454,184	484,728	1,938,910
Non-Federal Share	121,252	121,252	121,252	242,504	121,252	363,756	121,254	485,010
Total Planned	605,980	605,980	605,980	1,211,960	605,980	1,817,940	605,980	2,423,920
Actual Incurred Cost								
Federal Share	420,153	420,153	331,481	751,634	547,545	1,299,179	428,937	1,728,116
Non-Federal Share	29,456	29,456	131,875	161,332	151,972	313,304	100,629	413,933
Total Incurred Costs	449,609	449,609	463,356	912,966	699,517	1,612,483	529,566	2,142,049
Variance								
Federal Share	64,575	64,575	153,247	217,822	-62,817	155,005	55,789	210,794
Non-Federal Share	91,796	91,796	-10,623	81,172	-30,720	50,452	20,625	71,077
Total Variance	156,371	156,371	142,624	298,994	-93,537	205,457	76,414	281,871

Baseline Reporting Quarter	Yr. 2			
	Q5		Q6	
	10/1/10 - 12/31/10		1/1/11 - 3/31/11	
	Q8	Total	Q8	Total
Baseline Cost Plan				
Federal Share	323,403	2,262,313	323,402	2,585,715
Non-Federal Share	80,835	565,845	80,834	646,679
Total Planned	404,238	2,828,158	404,236	3,232,394
Actual Incurred Cost				
Federal Share	593,386	2,321,502		2,321,502
Non-Federal Share	191,601	605,534		605,534
Total Incurred Costs	784,987	2,927,036	0	2,927,036
Variance				
Federal Share	-269,983	-59,189	0	264,213
Non-Federal Share	-110,766	-39,689	0	41,145
Total Variance	-380,749	-98,878	0	305,358

MILESTONE STATUS

ID	Title/Description	Planned Completion Date	Actual Completion Date	Milestone Status
1.0	Project Management			
	Project management plan	Nov-09	Dec-09	
	Briefings & reports	Mar-11		Ongoing
2.0	Technology Transfer and Outreach			
	Upload geodatabase of water information to map	Mar-10	Mar-10	Reported in Q1 2010 report
	Hold project review meeting in the form of presentations/poster session at ICSE-sponsored unconventional fuels conference	May-10	Apr-10	Reported in Q2 2010 report
	Complete addition of research materials from each task listed below to online digital repository	May-10		200 documents are entered, but collection does not include materials from every task
	Implement interactive map usage tracking or determine that it is not feasible	Jun-10	Jun-10	Reported in Q2 2010 report
	Advisory board meeting	Jun-10	Apr-10	Reported in Q2 2010 report
	Deploy updated web mapping software	Jul-10	Sep-10	Deployment cancelled due to departure of employee
	Upgrade Dspace platform for digital repository	Aug-10	Aug-10	Reported in Q3 2010 report
	Standardize and improve map attribute information	Jan-11		Cancelled due to departure of employee
	Completion of student research experiences	Mar-11		No students participated in research over the summer, so this milestone will not be met
	Tech transfer workshop, conference, & forums	Mar-11		
	Hold final project review meeting in format determined jointly by DOE/NETL and ICSE	Mar-11		

ID	Title/Description	Planned Completion Date	Actual Completion Date	Milestone Status
3.0	Clean Oil Shale & Oil Sands Utilization with CO2 Management			
3.1	Macroscale CO2 analysis			
	Identify & collect experimental, literature, & simulation data on GHG emissions from process heaters	Mar-10	Mar-10	Reported in Q2 2010 report
	Identify or develop appropriate tool for predicting life-cycle GHG emissions from a given technology	Sep-10	Nov-10	Reported in this quarterly report
3.2	Flameless oxy-gas process heaters for efficient CO2 capture			
	Preliminary report detailing results of skeletal validation/uncertainty quantification analysis of oxy-gas combustion system	Nov-10		Delayed due to coding issues
4.0	Liquid Fuel Production by In-Situ Thermal Processing of Oil Shale/Sands			
4.1	Development of CFD-based simulation tool for in-situ thermal processing of oil shale/sands			
	Implementation of correct geometry representation in Star-CCM+	Jun-10		Completion scheduled for first quarter of 2011
	Implement submodels for pyrolysis, porosity development, etc. that provide a stable solution	Nov-10		Change milestone? See Subtask 4.1 summary
4.2	Basin-wide characterization of oil shale resource in Utah & examination of in-situ production models			
	Select dataset for use in validation/uncertainty quantification of in-situ production modeling	Mar-10		Unlikely to complete due to lack of industrial support for sharing data
	Develop models with preliminary geomechanics & reactions	Jun-10	Jun-10	Reported in Q2 2010 report
	Revise/revisit the P-4 core description, adding XRF and isotopic work	Dec-10	Oct-10	Reported in this quarterly report; summary report to be issues next quarter
	Describe one complete core, including XRF and isotopic work	Dec-10	Oct-10	Reported in this quarterly report; summary report to be issues next quarter
	Complete a regional cross section and synthesis of the four described cores (two cores have been completed to date)	Mar-11		

ID	Title/Description	Planned Completion Date	Actual Completion Date	Milestone Status
4.3	Multiscale thermal processing (pyrolysis) of oil shale			
	Complete pyrolysis experiments at two different scales	Feb-10	Mar-10	Reported in Q1 2010 report
	Complete mass balances for oil/gas/coke at different scales	Apr-10	Apr-10	Reported in this quarterly report
	Develop preliminary kinetic model for oil shale pyrolysis	Jun-10	Sep-10	Reported in Q2 2010 report & in paper manuscript
	Develop compositional representation of shale oils	Sep-10	Nov-10	Reported in this quarterly report
	Design experiments for performing pyrolysis under stress	Nov-10	Dec-10	Reported in this quarterly report
4.4	Effect of oil shale processing on water compositions			
	Complete preliminary analysis of process water, including some tables of aqueous phase organic species concentrations	Nov-10	Nov-10	Reported in this quarterly report
	Determine compositional impact on reservoir scale of soluble pyrolysis products	Dec-10		Will be reported next quarter
4.5	Pore scale analysis of oil shale/sands pyrolysis			
	Perform XMT/XNT analysis of samples of pyrolysis products at different temperatures	Jun-10	Jun-10	
	Model pore network structure at different heating rates to determine porosity changes	Sep-10	Oct-10	Delayed because samples not received from Subtask 4.3
	Use multiphase LB model to analyze fluid penetration into porous samples & to provide transport information such as connectivity, conductivity, & permeability	Dec-10	Dec-10	
4.6	Kerogen/asphaltene/mineral matrix: structure & interactions			
	Develop 3D models of kerogen & asphaltenes based on existing 2D models	Mar-10	Mar-10	Reported in Q1 2010 report

ID	Title/Description	Planned Completion Date	Actual Completion Date	Milestone Status
	Calculate interaction energies between organic components & mineral matrix using 3D models	Sep-10	Sep-10	Reported in Q3 2010 report
	Correlate spectroscopic data of isolated & absorbed 3D models, establish sensitivity to model structural features	Nov-10	Nov-10	
5.0	Environmental, Legal, Economic, & Policy Framework			
5.1	Land & resource management issues relevant to deploying in-situ thermal technologies			
	Detailed outline & abstract addressing land & resource management issues	Sep-10	Sep-10	
5.2	Policy analysis of water availability & produced water issues associated with in-situ thermal technologies			
	Detailed outline & abstract addressing produced water issues	Aug-10	Sep-10	
6.0	Economic & Policy Assessment of Domestic Unconventional Fuels Industry			
6.1	Engineering process models for economic impact analysis			
	Identify & describe selected scenarios & methodology applied to obtain associated upstream supply costs	Feb-10	Feb-10	
	Deliver upstream supply costs & listing of materials, equipment & services needed for facility construction & on-going operations & maintenance for each scenario	May-10	Jun-10	Spreadsheet of results included as attachment with Q2 2010 report
	Upload all models used & data collected to repository	Oct-10		Change from vertical to horizontal drilling has delayed completion
6.2	Policy analysis of the Canadian oil sands experience			
	Preliminary report addressing differences between U.S. & Canada in terms of taxes and royalties levied on production & in downstream/marketing challenges (to be incorporated into final report)	Jun-10	Jun-10	Included as appendix to Q2 2010 report

ID	Title/Description	Planned Completion Date	Actual Completion Date	Milestone Status
6.3	Market assessment report			
	Identify & describe criteria used to select scenarios for further study	Dec-09	Dec-09	Included as appendix to Q4 2009 report
	Identify & describe methodology applied to assess impact of downstream market conditions on potential revenue of upstream scenarios	Feb-10	Feb-10	Reported in Q1 2010 report
	Describe methodology & preliminary results of supply cost analysis for one scenario, including effect of system shocks or input variability	Apr-10	Dec-10	Will be released with rest of draft Market Assessment
	Deliver assessment of impacts to revenue corresponding to each scenario	May-10	Jun-10	Included as appendix to Q2 2010 report
	Preliminary report summarizing first three sections of Market Assessment (role of unconventional fuels in current energy climate; role of policy & government, role of externalities & public perception	Sept-10	Dec-10	Reported in this quarterly report

NOTEWORTHY ACCOMPLISHMENTS

For Subtask 4.5, the single component multiphase flow He-Chen-Zhang LBM model has been extended to incorporate fluid-solid interaction forces and has been applied to the simulation of percolation in actual XMT images of pore network structures for Athabasca and Sunnyside oil sand samples.

PROBLEMS OR DELAYS

For Subtask 3.2, the V/UQ analysis was delayed by coding issues, some of which have been resolved and some of which require further work. The code stability problem has been resolved as evidenced by the oxy-gas simulation results included in this report. The ability to include swirl number as a boundary condition and to incorporate flamelets-type reaction models requires further coding.

Researchers in Subtask 4.1 have been delayed in the implementation of a correct geometry representation in Star-CCM+ due to the many difficulties in creating a complex geometry that would best represent the experimental domain of the Red Leaf trial experiment. The completion of this milestone has been delayed until next quarter.

Subtask 4.5 researchers are continuing to look for funds to purchase a Nano CT instruments that will be required to characterize oil shale samples at the nano scale.

With Subtask 4.6, the only problem is the lack of experimental data for the comparison with the calculated results. This problems will be resolved in the next phase of the project with the recently acquired Skyline 16 core. However, it takes time for the processing of the core, so work will need to begin soon.

The Subtask 6.1 deliverable of a Topical Report describing process models used has been delayed due to the reworking of the in situ unconventional fuel scenarios and to scenario-to-scenario inconsistencies. Once this accuracy checking is completed, the Topical Report can be finalized.

Subtask 6.2 had several setbacks this quarter: (1) legal research and draft sections of the Oil Sands Topical Report were lost when a computer laptop containing the research and report was stolen from a Subtask 6.2 researcher's home in December 2010, and (2) two post-doctoral legal fellows working on the Topical Report terminated their employment with ICSE in November and December respectively. Reconstruction of the lost research and writing is expected to delay completion of the Topical Report by approximately ten weeks, until March 2011.

RECENT AND UPCOMING PRESENTATIONS/PUBLICATIONS

- C. L. Lin, J. D. Miller, C. H. Hsieh, P. Tiwari and M. D. Deo, "Pore scale analysis of oil shale pyrolysis by X-ray CT and LB simulation." Submitted for publication in the Proceedings of the 6th World Congress on Industrial Process Tomography, Beijing, China, September 2010.
- J. H. Bauman and M. D. Deo, "Simulation of a rubblized oil shale surface pyrolysis process," 30th Oil Shale Symposium, Colorado School of Mines, Golden, CO, October 18-20, 2010.
- J. H. Bauman, P. Mandalaparty, P. Tiwari, and M. D. Deo, "A low CO₂ hybrid in situ oil shale liquid production process," 30th Oil Shale Symposium, Colorado School of Mines, Golden, CO, October 18-20, 2010.
- L. Birgenheier and M. Vanden Berg, "Detailed geologic characterization of the Upper Green River Formation, Uinta Basin, UT," 30th Oil Shale Symposium, Colorado School of Mines, Golden, CO, October 18-20, 2010.
- P. Tiwari and M. D. Deo, "The effect of pressure on oil shale thermal treatment," 30th Oil Shale Symposium, Colorado School of Mines, Golden, CO, October 18-20, 2010.
- J. H. Bauman and M. D. Deo. Parameter space reduction and sensitivity analysis in complex thermal subsurface production processes. Accepted for publication in *Energy and Fuels*.
- K. P. Tiwari and M. Deo, "Detailed kinetic analysis of oil shale pyrolysis TGA data." Accepted for publication in *AIChE Journal*.
- J. H. Bauman and M. D. Deo, "Relationship between kinetic and flow parameter representations in complex in situ reactive processes," AIChE Annual Meeting, Salt Lake City, UT, November 7-12, 2010.
- K. E. Kelly, T. Ring, J. Wilkey, B. Castro, A.F. Sarofim, and D.W. Pershing, "Opportunities for oxyfiring to reduce upstream life-cycle greenhouse gas emissions from transportation fuels," AIChE Annual Meeting, Salt Lake City, UT, November 7-12, 2010.
- B. Isaac, M. Hradisky, P. Smith, "Development of CFD-based simulation tools for in-situ thermal processing of oil shale/sands," AIChE Annual Meeting, Salt Lake City, UT, November 7-12, 2010.

- P. Tiwari and M. Deo, "Thermal gravimetric – mass spectrometry analysis of oil shale," AICHE Annual Meeting, Salt Lake City, UT, November 7-12, 2010.
- C. L. Lin, J. D. Miller, and C. H. Hsieh. "Flow simulation with the Lattice Boltzmann method in 3D porous structures of pyrolyzed oil shale cores using multiscale X-Ray CT imaging," AICHE Annual Meeting, Salt Lake City, UT, November 7-12, 2010.
- C.L. Lin, A.R. Videla and J.D. Miller. "Advanced 3D multiphase flow simulation in porous media reconstructed from X-ray micro tomography using the He-Chen-Zhang Lattice Boltzmann Model," *Flow Measurement and Instrumentation*, 21 (2010) 255-261.
- I. S. O. Pimienta, A. M. Orendt, J. C. Facelli, and R. J. Pugmire, "Ab initio calculation and molecular dynamics simulation of asphaltenes." Submission to a journal in first quarter 2011.
- I. S. O. Pimienta, A. M. Orendt, R. J. Pugmire, J. C. Facelli, D. R. Locke, R. E. Winans, K. W. Chapman, and P. J. Chupas, "Three-dimensional structure of the Siskin Green River oil shale kerogen model: A computational study." Publication of manuscript has been delayed pending acquisition of experimental data.

REFERENCES

- ANL. (2009). The greenhouse gases, regulated emissions, and energy use in transportation (GREET) model, version 1.8c0. Retrieved from http://www.transportation.anl.gov/modeling_simulation/GREET/index.html.
- Coraggio, G. & Laiola, M. (2009). Combustion of NG and pulverized coal in a mixture of oxygen and RFG (IFRF. Doc. No F110/y/01). Pisa, Italy: International Flame Research Foundation.
- He, X. Chen, S., and Zhang, R. (1999). A lattice Boltzmann scheme for incompressible multiphase flow and its applications in simulation of Rayleigh-Taylor instability, *J. Comput. Phys.*, 152, 642-663.
- Lenormand, R, Touboul, E., Zarcone, C. (1988). Numerical methods and experiments on immiscible displacements in porous media. *J. Fluid Mech.*, 189, 165-87.
- Marle, C.M. (1981). Multiphase flow in porous media, Houston: Gulf Publishing Company.
- Siskin, M., Kelemen, S. R., Eppig, C. P., Brown, L. D., & Afeworki, M. (2006). Asphaltene molecular structure and chemical influences on the morphology of coke produced in delayed coking, *Energy & Fuels*, 20, 1227-1234.
- Taciuk, W. (2009). Test results relating to changes in oil yield and gas compositions of oil shale samples subjected to short and medium time and temperature exposure at atmospheric pressure, 29th Oil Shale Symposium, Golden, CO, October 19-21.

National Energy Technology Laboratory

626 Cochrans Mill Road
P.O. Box 10940
Pittsburgh, PA 15236-0940

3610 Collins Ferry Road
P.O. Box 880
Morgantown, WV 26507-0880

13131 Dairy Ashford, Suite 225
Sugarland, TX 77478

1450 Queen Avenue SW
Albany, OR 97321-2198

2175 University Ave. South
Suite 201
Fairbanks, AK 99709

Visit the NETL website at:
www.netl.doe.gov

Customer Service:
1-800-553-7681

